An atomistic introduction to anisotropic etching

M A Gosálvez[1], K Sato[1], A S Foster[2], R M Nieminen[2] and H Tanaka[3]

[1] Department of Micro-Nanosystem Engineering, Nagoya University, Nagoya 464-8603, Japan

[2] Laboratory of Physics, Helsinki University of Technology, PO Box 1100, 02015 HUT, Finland

[3] Denso Corporation, Showa-cho, Kariya, Aichi 448-8661, Japan

E-mail: mag@kaz.mech.nagoya-u.ac.jp

Abstract

This review-oriented paper presents a simplified model of anisotropic etching of crystalline silicon for the three principal orientations (1 1 1), (1 1 0) and (1 0 0), including their vicinal surfaces. The model combines pit nucleation and step flow with micromasking and diffusion phenomena in order to explain the major morphologic features and their changes with concentration. It also qualitatively explains the orientation and concentration dependence of the etch rate. We conclude that the shallow round pits on (1 0 0) and the elongated zigzag structures on (1 1 0), each of which constitutes the basic morphology of the corresponding surface, are actually the result of the same physical phenomenon, diffusion, disguised by a different underlying symmetry. It is also shown that the formation of hillocks on the two surfaces at different concentrations is a related process. We also describe and support the idea that the rotation of the triangular pits on (1 1 1) is due to a selective blocking mechanism by the etchant cations and explain how the formation of polygonal steps and/or step bunches on miscut (1 1 1) surfaces can occur as a result of diffusion phenomena and not only due to micromasking. Finally, the particular features of Cu as a micromasking agent are explained.

(Some figures in this article are in colour only in the electronic version)

1. Introduction

The main objective of this paper is to serve as an introduction to anisotropic wet chemical etching of crystalline silicon by presenting a simplified description of the process at the atomistic scale. It is meant to be of help for non-experienced students, researchers and application engineers who are exposed for the first time to the use of etching as part of their work, providing them with a basic understanding of the fundamental atomistic mechanisms involved. For the more experienced researcher, our perspective can be of interest as it tries to unify different features which appear somehow dispersed in the literature. At times, in an effort to remain consistent with the overall picture presented for the process, we

take some risks and some of the presented ideas will challenge some of the established views in the field.

Our point of view is atomistic, stressing the role of pit nucleation, which results from removing atoms at terrace sites and step flow, which is the result of atom removals at kink sites, typically scattered along the steps. However, the paper presents also features which can be categorized as mesoscopic, such as diffusion phenomena, where the reactants and/or products diffuse into or out of the regions where the reactions occur. The atomistic processes explain the most basic features of wet etching, namely, the low etching rate of the (1 1 1) surface as compared to any other orientation, while the mesoscopic processes explain the formation of step bunches on miscut (1 1 1) surfaces and of zigzag structures on the

(1 1 0) orientation. In addition, an important atomistic process, micromasking, is also considered. If present, it is responsible for the formation of both mesoscopic and macroscopic features such as the so-called 'noses' of the zigzag structures on (1 1 0) as well as the pyramidal hillocks that will appear on (1 0 0) and (1 1 0) at different concentrations.

Apart from the numerous details presented through the different sections, which can become rather technical and in some cases still need to be fully proved, the paper introduces the important concepts of pit nucleation, step flow, micro masking and diffusion transport in a unified manner. In this sense, the manuscript can be useful for starting students and starting application engineers who typically perceive anisotropic etching with a reductionist mind as a process which simply produces flat and shiny (1 1 1) surfaces when used in conjunction with masks. Typically, as soon as the students encounter some of the characteristic morphologies through the use of a microscope (such as the pits, the hillocks, the zigzags or the stepped side walls that are developed when the mask is slightly misaligned), they ask why these features occur. At that time, bringing out this document can help. Even though the students will not probably understand all the details, simply getting the information about the four key ingredients will satisfy their curiosity to a certain extent.

The description of anisotropic etching as a step-flow process in this paper is not a novel idea, neither is the explanation of some of the key features by using micromasking and diffusion phenomena. Probably, the main value of the paper is to provide a rather consistent account of etching by considering the three ingredients together.

The step-flow aspects of anisotropic etching can be traced back to the *in situ* STM observations by Allongue *et al* [1] and the theoretical exploration of the similarities between etching and growth by Elwenspoek [2]. Much of the experimental microscopy and spectroscopy carried out in relation to etching in the early and mid 1990s uses the concept of step propagation [3–5]. Following these pioneering works for etching, the idea of step flow matured during the late 1990s, resulting in the development of atomistic etching simulators that use step propagation in one way or another [6–9]. The first simulations of etching as a step-flow process were those from Flidr *et al* using the (kinetic) Monte Carlo method [6]. This and other subsequent papers from the same group [10–13] have not only stressed the importance of step propagation but have also explored possible mechanisms to explain the interaction between the steps in an effort to describe step bunching, a rather usual process during etching, as will be described in the paper. Earlier Monte Carlo [14–17] and cellular automata [18, 19] simulators did not recognize the importance of step flow. Today, their popular cellular automata descendants in engineering [20, 21] still completely disregard the role of kink propagation and step flow. In some sense, this introductory paper partly aims at reducing the conceptual gap by bringing closer the main ideas from fundamental research to the engineering community.

The concept of step flow was developed earlier in growth, starting with the classical paper by Burton, Cabrera and Frank [22], where growth is reduced to the propagation of existing steps, their nucleation (by island formation) and their annihilation (by merging the islands and terraces). The central

role of the kink sites as the actual locations where growth takes place has been stressed in numerous occasions (see, e.g. [23]). In etching, similar ideas were put forward by Elwenspoek who, based on the similarities to growth, pointed out the existence of a birth-and-spread mechanism and the importance of the kinks as one of the weakest sites for the removal of atoms [2].

In a similar manner, the importance of diffusion phenomena for explaining certain features of anisotropic etching is not a new idea of this paper. The use of stirring in order to assess the role of diffusion has been and still is a popular procedure. Early studies produced conflicting results where the etch rate of silicon in potassium hydroxide (KOH) was found to be only slightly affected by stirring [24, 25] while the etch rate in ethylene diamine pyrocatechol (EDP) [25, 26] and tetra methyl ammonium hydroxide (TMAH) [27] was affected more strongly. For the case of KOH, it was later found by Tan *et al* that the etch rate and apparent activation energy of (1 1 1) are consistently different when widely and closely separated masking patterns are used [28], in agreement with the observations in [25] and demonstrating that diffusion phenomena have an important role also in KOH. They reasoned that the time delay between the surface atomistic reactions and the transport of the reactants and/or products to the regions of consumption/production results into the formation of etchant depletion regions, thus affecting the etch rate. Later on, it has been shown both experimentally and theoretically—by means of atomistic simulations—that also the surface morphology of stepped (1 1 1) surfaces is strongly dependent on the formation of inhomogenous regions in the etchant directly in contact with the surface [12, 13]. More recently, the use of atomistic simulations has also shown that the zigzag structures characteristic of the morphology of (1 1 0) are mainly the result of the formation of inhomogeneities in the etchant [29]. In fair reflection of the accumulated experimental and theoretical evidence, this paper tries to emphasize the importance and the role of diffusion phenomena.

Also the use of micromasking as an essential mechanism for explaining certain surface morphologies during etching is by no means a novelty in this paper. Micromasking during etching refers to the presence of numerous, independent, simultaneous, small-scale, blocking locations on the silicon surface due to the formation of insoluble compounds or the deposition of relatively stable agents which do not react with the etchant, such as atoms, molecules or larger clusters whose size is well below the micron scale. As an example, the micromasking agents have been associated with the formation of hydrogen bubbles [30–33], polymerized residues, reaction products and/or SiO_2 precipitates [25, 33, 34], regrowth of silicon [34, 35], semipermeable silicate particles [36, 37] and (metal) impurities [30, 38–43]. Among all morphologic features which can only be explained by assuming the presence of micromasks, the most important are the pyramidal and trapezoidal hillocks appearing on Si(1 0 0) and Si(1 1 0), respectively (see section 4), and the so-called 'noses' of the zigzag structures appearing on exactly oriented (1 1 0) surfaces (section 4.1).

Although the idea of micromasking as due to impurities present in the etching bath is probably as old as etching itself, one can probably cite the study of an underlying correlation between pyramid formation and water quality and etchant
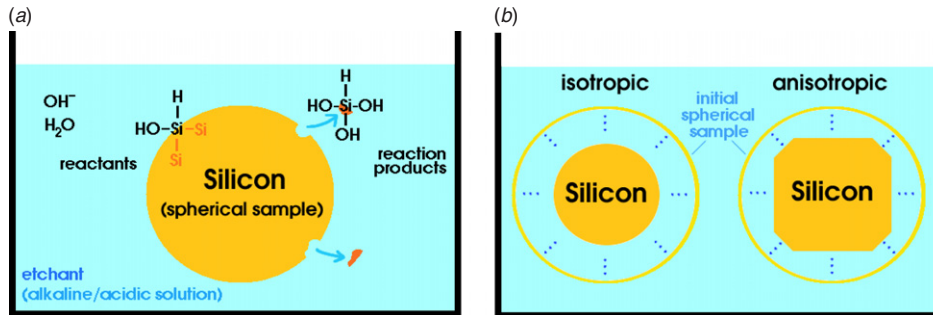
Figure 1. (*a*) Schematic illustration of the dissolution process during wet etching. (*b*) Wet etching can be isotropic or anisotropic. From [46] (figure 1).

purity by Campbell *et al* [30] as the first systematic study, even though Campbell and co-workers eventually focused primarily on the hydrogen bubbles as the source of micromasking. Also Landsberger *et al* [38] were among the first ones to point out that the etchant impurities are possibly precursors of the micromasks. Tanaka *et al* [42] and Gosálvez *et al* [43] have stressed the role of metal impurities as micromasking agents. For a more detailed overview of micromasking and the formation of hillocks, we refer to section 3 of [43].

More recently, a rather sophisticated three-dimensional network function model primarily based on step propagation and step formation has been presented [7, 44, 45]. Here, the simple birth-and-spread model of etching is decorated with a mathematically sounded Exponential Assembling technique where the total etch rate (or, actually, the square of it) for any surface orientation is obtained by summing the squares of the different rates associated with a few physical processes. In principle, other powers (or 'assembling exponents') can be considered. The approach leads to a phenomenological expression for the etch rate of any surface as a function of (i) one- and two-dimensional roughening parameters which account for kink and pit nucleation rates, respectively; (ii) step-flow velocities which describe step propagation for steps on $(1\,1\,1)$ and $(1\,0\,0)$ surfaces, and related miscuts; and (iii) the so-called 'mesoscopic shortcuts' which incorporate diffusion and micromasking effects. The present paper can be considered as an alternative presentation of the same physical mechanisms without making use of the three-dimensional network function model.

Since the paper targets at providing a simplified introduction to wet etching, the electrochemical features of the process are only briefly considered in section 2. For more details the reader is directed to [46] and references therein.

Similarly, we have left aside some of the very interesting and useful effects derived from the use of ionic and non-ionic surfactants [47–51] and other etchant additives such as isopropyl alcohol (IPA) [50, 52–54]. Typically, the surfactants have a beneficial effect on the surface roughness, smoothening the morphology, although in some cases some orientations are smoothened while others are roughened [51]. Generally, only the ionic surfactants (either cationic or anionic) affect positively the etch rate of $(1\,0\,0)$, increasing it [48, 49], in opposition to the non-ionic surfactants which typically result in an etch rate reduction [50, 51, 53]. Although not reported in [48, 49], the etch rate of $(1\,1\,0)$ presumably decreases after addition of the ionic surfactants in the same way as it

reportedly occurs for non-ionic surfactants [50, 51, 53]. These effects are believed to be partly due to the changes in the anisotropy of the resulting etchant, where Si$(1\,1\,0)$ becomes slower than Si$(1\,0\,0)$ [51], and partly due to changes in the wetting characteristics of the resulting etchant [48, 49]. In most cases, the addition of the surfactants leads to smaller droplet contact angles and thus larger wetting ability [48, 49]. This enhances hydrogen bubble detachment and promotes diffusion of the reactants and/or products in the boundary layer.

Finally, the paper considers some aspects related to the influence of the etchant cations, i.e., K$^+$ for KOH and TMA$^+$ for TMAH. In doing so, the paper opens certain connections to some electrochemical aspects of etching.

The paper is organized as follows: in section 2 we present a simplified etching model for $(1\,1\,1)$ by introducing pit nucleation and step propagation as the basic processes as well as a minimum number of definitions necessary for further discussion. We then describe the formation of pits on this surface and how their shape changes with concentration. Finally, we describe the typical morphologies for $(1\,1\,1)$ miscut surfaces, which are easily understood using the underlying step propagation process. In section 3 we consider the effects from diffusion which lead to the formation of inhomogeneities in the etchant, resulting into step bunching on miscut $(1\,1\,1)$ surfaces. In section 4 we describe how the inhomogeneities produce the zigzag structures on $(1\,1\,0)$ and the dramatic effects that micromasking can have on the morphology of $(1\,0\,0)$ and $(1\,1\,0)$. Also the similarities between the effects of diffusion on these two surfaces are brought out. In section 5 we explain the changes in the surface morphology and etch rate due to the addition of metal impurities, which can act as micromasking agents. Finally, in section 6 we consider the special features of surfaces such as $(1\,1\,3)$ and $(3\,3\,1)$ and we abstract on the overall behavior of the etch rate as a function of orientation and concentration for a generic etchant. In section 7 we summarize our conclusions.

2. Anisotropic etching as a step-flow process

Anisotropic wet chemical etching of crystalline silicon consists of the removal of material from the surface of silicon due to a complex reaction between the silicon atoms, the water molecules, the OH$^-$ ions and the etchant cations present in an alkaline/acidic water solution (the etchant), as schematically outlined in figure 1(*a*). The fact that the initial shape of
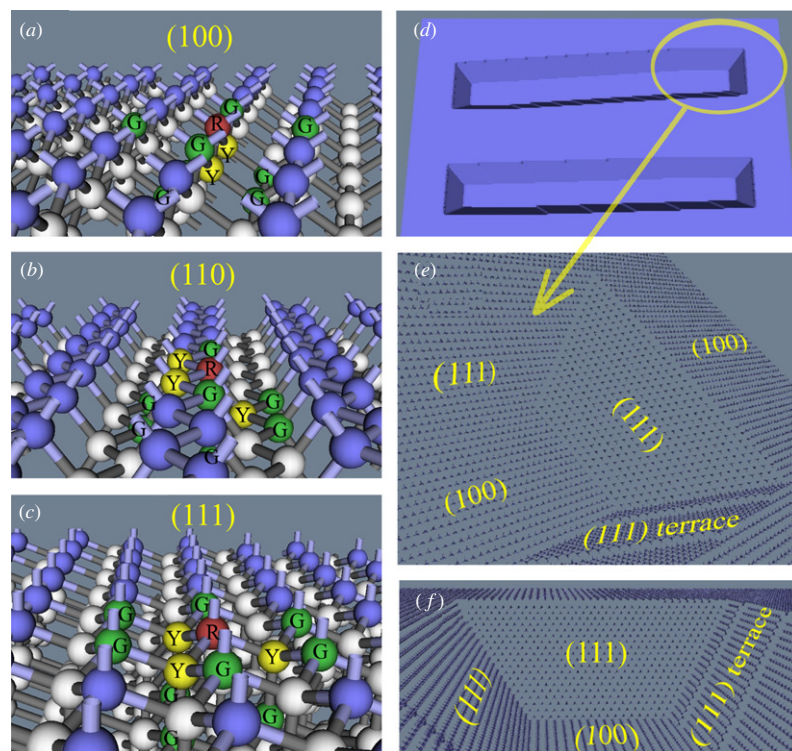
Figure 2. Link between microscopic structure and macroscopic anisotropy during etching. (*a*)–(*c*) Typical atoms on each principal surface are shown in red color (R) and their first (second) neighbors in yellow (Y) (green (G)); (*d*) Example of a 3D etched structure on a (1 0 0) wafer (misaligned trenches); (*e*)–(*f*) Details of the region highlighted in (*d*), showing the slow etching (1 1 1) surfaces.

the crystal usually changes during exposure, as shown in figure 1(*b*), implies that the etching process is anisotropic, i.e. it is slower along certain crystallographic directions than along others. More properly, the anisotropy of the etching process refers to the orientation dependence of the etch rate, which is defined as the ratio of the distance advanced by the surface to the time of exposure.

The macroscopic anisotropy or orientation dependence of the process originates from the fact that the removal of the surface atoms is a site-dependent process at the microscopic scale [6, 9, 55]. This simply means that different surface sites (see figures 2(*a*)–(*c*)) show different reaction rates, ultimately resulting from different energy barriers for the removal of each surface atom [56]. As an example, a surface such as (1 1 1), where each atom is tightly bound to three neighbors, typically shows a slow etch rate whilst a surface such as (1 0 0), where each atom is linked to only two neighbors, typically has a larger etch rate (figures 2(*a*)–(*c*)). The anisotropy of the process is a most valuable property as it provides a cost-effective procedure to shape 3D micromachined structures by making use of the difference between fast and slow etching orientations (figures 2(*d*)–(*f*)).

The removal of the surface atoms is a complex process that involves both chemical and electrochemical reactions [57]. These are distinguished by the fact that the latter involve the participation of free charge carriers, giving rise to measurable currents and allowing for the possibility of controlling the etching process with a biasing potential [3, 58–62]. As shown in figure 3, the etching process takes place through sequential oxidation and etching reactions. The chemical (figure 3(*a*)) and electrochemical (figure 3(*b*)) reaction routes

provide two alternative mechanisms for the oxidation of the hydrogen-terminated sites before the actual removal of the resulting hydroxyl-terminated silicon (figure 3(*c*)). The fact that the surface of silicon is predominantly H-terminated during anisotropic etching [55, 63, 64] is simply explained by acknowledging that the oxidation step is the rate-limiting process. Once the substitution of H by OH has taken place, a fast sequence of chemical steps (represented as 'etching' in the figure) leads to the removal of the silicon atom (as a $Si(OH)_4$ product). This triggering effect of the OH ligand is attributed to the difference in electronegativities between Si and O, resulting in the polarization and weakening of the backbonds, which, as a result, become more vulnerable to further attack. For more details about the electrochemistry of anisotropic etching see [46] and references therein, especially [25, 58–61] of this work.

2.1. Simplified etching model for exact (1 1 1)

As mentioned in section 1, two basic mechanisms describe the etching process at the microscopic scale: pit nucleation and step propagation, as depicted in figure 4. This is best pictured on the stable (1 1 1) surface, where the removal of a three-bonded atom is a very unusual process. When it occurs, it leaves behind three more reactive sites with higher probability to be removed. The removal of these sites soon leads to the formation of steps, eventually growing longer and serving as a separation boundary between the lower and upper terraces. As a result of the three-fold symmetry of this surface (due to the three-fold bonding configuration of its atoms), triangular etch pits are formed. In this way, the removal of a three-bonded
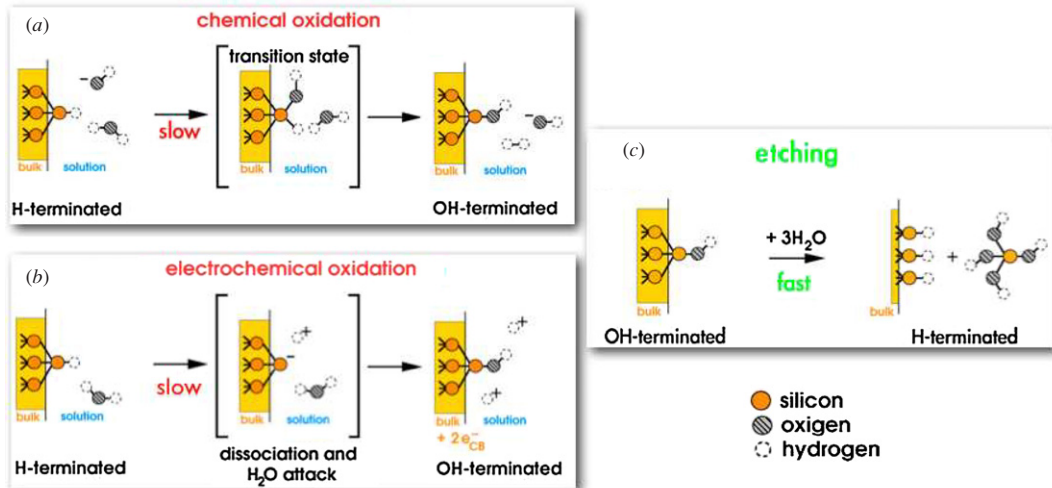
Figure 3. Cartoon-like description of the sequential oxidation and etching reactions taking place during etching. Only the nearest underlying bulk atoms in the neighborhood of the surface site are depicted. From [46] (modification of figures 5, 6 and 7).
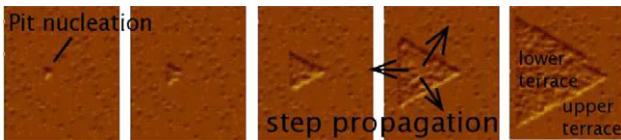
Figure 4. Pit nucleation and step propagation on (1 1 1). Simulation.

terrace atom is said to nucleate a pit, which then grows in-plane by virtue of step propagation.

Step propagation itself is typically an unzipping process resulting from kink propagation, as pictured in figure 5. In a perfect step between two (1 1 1) terraces, the step sites are rather stable (although more reactive than the previous terrace sites). When one of the step sites is removed, two reactive kink sites are created. When either kink is removed, a new kink is left behind. Thus, etching proceeds by sequentially removing the next kink off from the step, a process that is observed as kink propagation or unzipping of the step.

Before one can go on and discuss more features of the etching process, it is necessary to agree on a few definitions and some notation. Taking into account that the surface of silicon

is typically H-terminated in the experiments [55, 63, 64], the three-bonded, single-hydrogen-terminated atoms at the (1 1 1) terraces are referred to as terrace monohydrides (TM), where 'monohydride' refers to the number of H-terminations being one (see figure 6(a)). Similar definitions are found for other usual surface sites [5]. For instance, there are two types of stable steps between (1 1 1) terraces, depending on the etchant concentration. At low concentration, the steps are made of three-bonded, single-hydrogen-terminated atoms referred to as Step Monohydrides (SM), as shown in figure 6(b). At high concentration, the steps contain two-bonded, double-hydrogen-terminated atoms named step dihydrides (SD), as shown in figure 6(c). As a matter of fact, one can distinguish between two types of SD sites: horizontal and vertical step dihydrides (HSD and VSD, respectively), as shown in figures 6(c)–(d). This depends on whether the dihydride (made by the silicon atom and the two hydrogens) lies on a plane that is (almost) horizontal or (almost) vertical with respect to the terrace plane, which is assumed horizontal. The VSD sites appear after the removal of the HSD atoms and, reversely, the HSD sites appear after removing the VSD atoms.
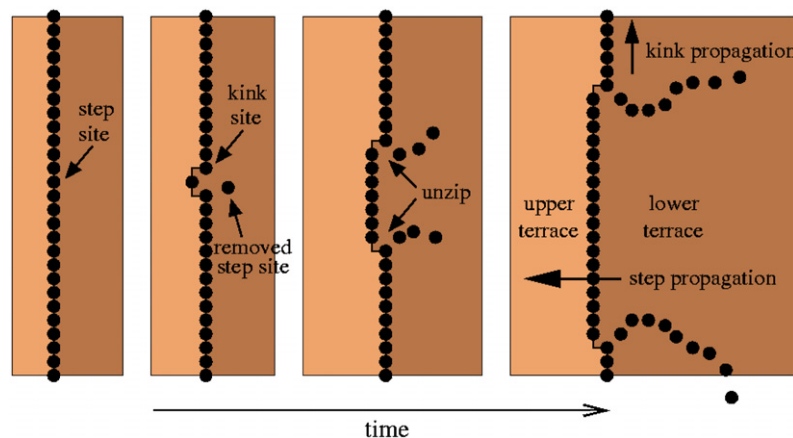
Figure 5. Cartoon-like description of step propagation as an unzipping process on (1 1 1).
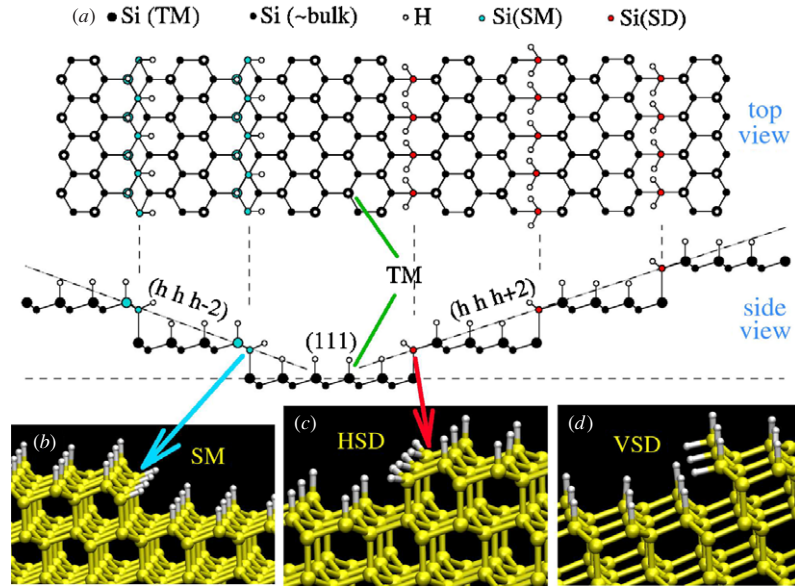
Figure 6. Identification of the typical surface sites appearing on (1 1 1).
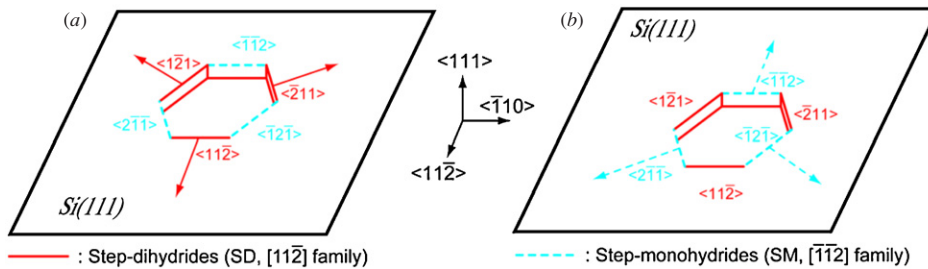
Figure 7. The $[1\,1\,\bar{2}]$ and $[\bar{1}\,\bar{1}\,2]$ step families on (1 1 1).

Due to the three-fold symmetry of the (1 1 1) surface, which is inherited from the three-fold bonding configuration of the TM sites, three equivalent SD steps appear on the (1 1 1) surface, as depicted in figure 7(*a*). The steps, which are referred to according to their in-plane normals $\langle 1\,1\,\bar{2}\rangle$, $\langle 1\,\bar{2}\,1\rangle$ and $\langle\bar{2}\,1\,1\rangle$, form the $[1\,1\,\bar{2}]$ step family. Similarly, there are three equivalent SM steps on (1 1 1), which are referred to as the $[\bar{1}\,\bar{1}\,2]$ family, as shown in figure 7(*b*).

As figure 8 shows, the ideal (1 1 0) and (1 0 0) surfaces are composed of SM and SD sites, respectively. According to the figure, (1 1 0) and (1 0 0) can be considered as the limiting cases of two major families of stepped (1 1 1) surfaces. On the one hand, the $(h\,h\,h-2)$ family with $h \geqslant 2$ which shows (1 1 1) terraces separated by SM steps. On the other hand, the $(h\,h\,h+2)$ family with $h \geqslant 0$ which has the terraces separated by SD steps. The general notation $(h\,h\,h\pm 2)$ for the two families is subjected to division by a common multiplier of the resulting (hkl) values. As an example, for $h = 4$ one gets (442) and (446), which convert to (221) and (223), respectively, after dividing by 2. From the perspective of (1 1 1) stepped surfaces, (1 1 0) is a SM-stepped surface with no terraces. Similarly, (1 0 0) is a SD-stepped surface, also without terraces.

The previous classification of the surface sites into TM, SM and HSD/VSD, being primarily based on the number of first neighbors (through the number of back bonds), is actually insufficient considering the fact that the site-specific etch rates are known to depend also on the number of second neighbors and not only on the number of first neighbors [9]. The classification is, however, deeply rooted in the field and, thus, it is convenient to use it as much as possible if there is no real need to be more specific. According to a more sophisticated model of etching that takes into account steric hindrance of the H/OH termination of the surface [43], a better classification of the surface sites would be based on the use of three integers $\left(n_1; n_2^d, n_2^i\right)$ denoting the number of first (n_1) and second $\left(n_2 = n_2^d + n_2^i\right)$ neighbors for each site, where the second neighbors are split into direct $\left(n_2^d\right)$ and indirect $\left(n_2^i\right)$.

As will become apparent throughout the rest of this paper, it is essential to keep a clear picture of the ideal (1 1 1), (1 1 0) and (1 0 0) surfaces composed of TM, SM and SD sites, respectively.

2.2. Etch pit shape dependence on etchant concentration

The triangular pits of figure 4 are formed on (1 1 1) as a result of the three-fold symmetry of this surface and the difference between the reaction rates of the different sites: the terrace sites are very stable, the step sites are stable and the kink sites are very reactive. Due to the existence of the two crystallographic step families, $[1\,1\,\bar{2}]$ and $[\bar{1}\,\bar{1}\,2]$, which are stable at different concentrations, also the shape of the etch pits is found to depend on the concentration. For instance, at low concentration, where the SM steps are stable and the SD steps are reactive, the pits are typically triangular, delimited
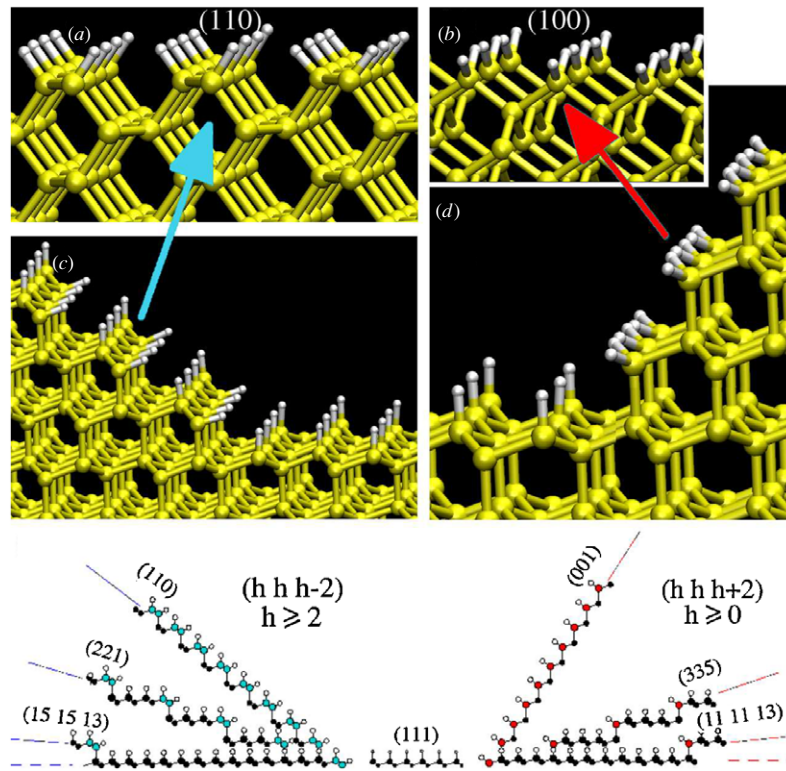
Figure 8. (1 1 0) and (1 0 0) as limiting examples of stepped (1 1 1) surfaces.
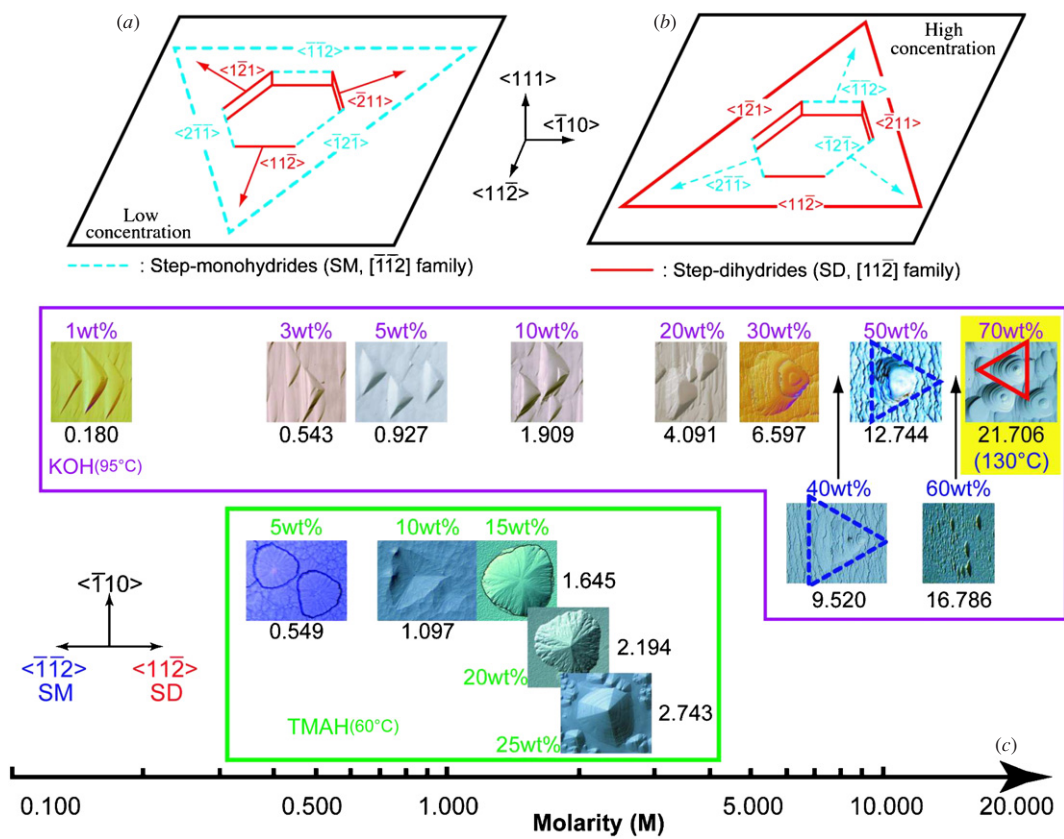
Figure 9. Etch pit shape dependence on etchant concentration. Frame (*c*) from [66] (figure 3) with permission © 2006 IEEE.
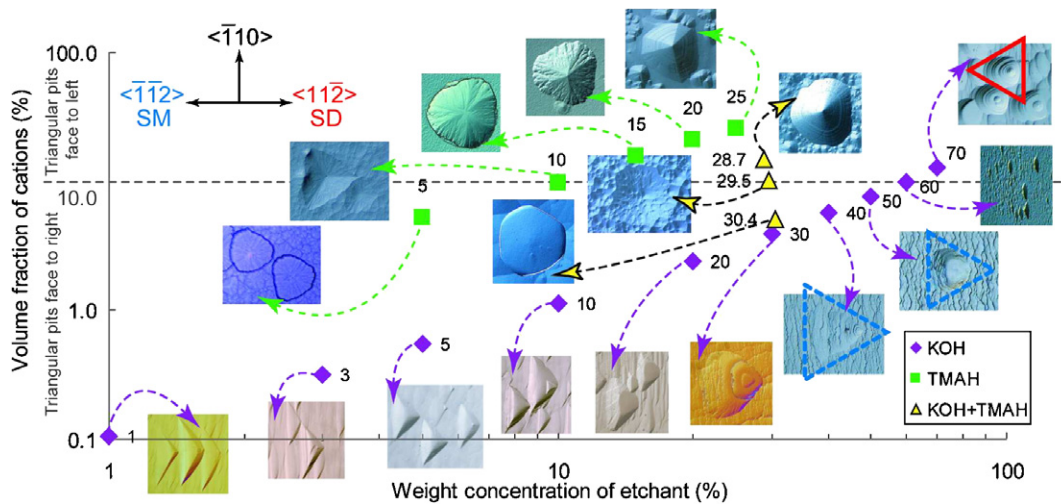
Figure 10. Cation volume concentration as a function of weight concentration for three different etchants. From [66] (figure 5) with permission © 2006 IEEE.

by SM sites, as sketched in figure 9(*a*). At high concentration, where the situation is the opposite with the SD steps being stable and the SM steps reactive, the pits are also triangular but they are rotated 60° with respect to the previous pits. This corresponds to the fact that now the pits are delimited by the SD sites (figure 9(*b*)). Figure 9(*c*) shows how this pit rotation occurs in the experiments for two different etchants: KOH and TMAH. At intermediate concentrations, the pits can be hexagonal, reflecting the fact that both step families are equally stable/reactive against etching. For intermediate, low- or high-biased concentrations, the hexagonal shape gradually becomes triangular.

Flidr *et al* have studied this change in the shape of the pits as a function of the relative stability/reactivity of the different sites using kinetic Monte Carlo simulations [6]. Although not directly linking their results to specific values of the concentration, they found that, when the VSDs are more reactive than the SMs by two orders of magnitude, the pits are clearly triangular and delimited by SMs. In the opposite case, the pits have rotated 60° and exhibit the more stable VSDs. When the difference in reactivity is reduced to ten times, the triangular pit corners become blunt, and the pits start to resemble the hexagonal shape. When the two site types have equal reactivity, the pits become hexagonal.

Since wet etching takes place in water solutions, it is natural to expect that the previous pit rotation with concentration should correlate with the pH value, or, what is equivalent, with the pOH. Indeed, there are many wet etching studies where a number of variables are presented as a function of the pH value [65]. However, figure 9 shows that the molarity (which measures the concentration of hydroxyls OH in the solution) plays no role as there is no correlation between the molarity values quoted for KOH and TMAH, and the rotation of the pits.

As an alternative to the molarity, the size of the cations in the different etchants has been proposed as an explanation [66]. This is based on the assumption that the cations can affect the etch rate by physically or chemically blocking the silicon surface during etching. If the cations prefer to chemically link more actively to the SD sites than to the SM sites, a larger

volume of cations in the etching solution (due to an increase in the etchant concentration) will lead to a lower etching rate for the SD sites, explaining the rotation of the pits in any etchant.

We have planned to perform *ab initio* calculations in order to understand the details of the interaction between the different cations (such as K^+ and TMA^+) and the H-terminated and/or OH-terminated step sites. According to preliminary results, the hydroxyls (OH^-) favor H-substitution (similar to the substitution shown in figure 3) at the SD steps better than at the SM steps and, as a result, the cations (K^+, TMA^+, . . .) are presumably attracted to the SD steps (due to the partial negative charge of the Oxygen atom in the hydroxyl group). This stabilization of the SD sites is further promoted by increasing the etchant concentration, due to the increased presence of both cations and hydroxyls. The size of the cation plays a role by directly blocking a larger or smaller region of the step, thus affecting the step reactivity.

A similar adsorption mechanism has been pointed out by Zubel and Kramkovska [53] for the TMA^+ ions and isopropanol (IPA) particles in order to explain the typical reduction in the etch rate with the addition of IPA. Their absorption mechanism, however, does not consider the component of selectivity due to the chemical interaction with the hydroxyls adsorbed on the surface.

The previous selective cation blocking mechanism has been tested experimentally [66]. Skipping the details, figure 10 shows that the direction of the etch pits rotates at approximately 10% of the volume concentration of cations in three different etchants (TMAH, KOH and a mixture). This demonstrates that the cations have a preference to chemically block the SD sites so that SD removal is strongly suppressed when the cation volume fraction reaches a value of about 10%.

The mechanism of selective blocking by the etchant cations can also explain why the etch rate of Si(1 1 0) increases more than that of Si(1 0 0) with increasing concentration in KOH [67, 68]: (1 0 0) has a large surface fraction of SD sites and etching of these sites is suppressed, whilst (1 1 0) has a large fraction of SM sites, which are not so dramatically affected. In addition, blocking can explain why the etch rate of Si(1 0 0) strongly decreases in TMAH with small increments
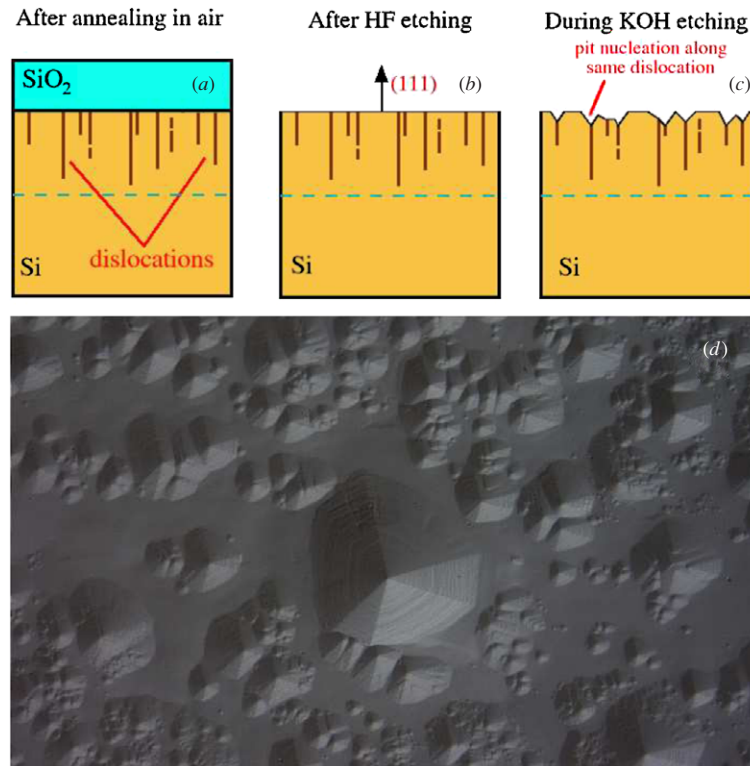
Figure 11. Formation of deep pits on (1 1 1) due to dislocations. Experimental image from Sato Laboratory, Nagoya University (unpublished).

in the concentration: the larger size of the TMA+ cation (as compared e.g. to the K+ cation of KOH) will block and affect the etching of the SDs more effectively.

Note that the triangular/hexagonal pits appearing on (1 1 1) are very shallow under typical experimental conditions, in contrast with the pits shown in figure 10, the reason being that pit nucleation is typically a very rare process. As a result, it is typically difficult to observe the pits, except by using time-consuming AFM and/or STM microscopy. It is however possible to visualize the pits using more conventional, less-expensive optical microscopy by previously preparing the sample to enable an increased amount of pit nucleations, as done for figure 10. This is done by heavily oxidizing the wafer through simple exposure to air for 20 h at about 1100 °C [69]. This process results into the growth of a layer of several microns of silicon oxide (SiO_2), whose lattice parameter is slightly larger than that of Si (figure 11(a)). As a result of the lattice mismatch, dislocations are induced into the Si crystal within a depth of 1–2 μm from the contact with the SiO_2 layer. After the removal of the oxide layer by HF etching (which does not dissolve silicon itself), the dislocation-rich region of silicon rises to the surface (figure 11(b)). At this stage, anisotropic etching with an alkaline etchant will result into deep pits as shown in figures 11(c)–(d). This occurs because pit nucleation is enabled to occur layer after layer along the dislocations, until the dislocations are finished. Once the dislocation region has been etched away, the pits become shallow again.

2.3. Morphology of misoriented (1 1 1)

When we move away from the exact (1 1 1) orientation, different surface morphologies can be observed as a result

of the concentration and orientation dependence of the step-flow process. The analysis is simplified by considering the two major miscut families introduced in figure 8. At low concentration, ($h\,h\,h − 2$) misaligned surfaces initially containing SM steps preserve their overall appearance during etching due to the intrinsic stability of the steps, as shown in figures 12(b) and (d). However, the ($h\,h\,h + 2$) surfaces, which initially contain the reactive SD steps, suffer a transformation, becoming polygonal as the stable SM steps are dug out. This can be seen in figures 12(c) and (f). In this case, the overall polygonal step morphology remains during additional etching after the initial transformation has taken place. For orientations initially containing both types of steps, the etched morphology can be understood by considering a mixture of the two previous extreme cases. Figure 12 has been obtained using kinetic Monte Carlo simulations similar to those reported in [6]. The site-dependent rates were assigned according to the number of first and second neighbors (n_1 and n_2), as described in table 1.

An important ingredient for the formation of the polygonal steps is the existence of an external stabilizing agent that pins (at least momentarily) the atoms at the convex polygonal tips. These atoms are characterized by lying on double-kink sites (see figure 13). Without such pinning, the shape of the steps deviates from polygonal, becoming atomistically random, although macroscopically linear, as shown in figure 12(g). The actual nature of the pinning process is an important issue. In section 5 we consider the particular case of metal impurities such as Cu, which according to our results can have a particularly active role in stabilizing certain surface sites. In addition, the role of the etchant cations as selective pinning agents will be clarified in the future.
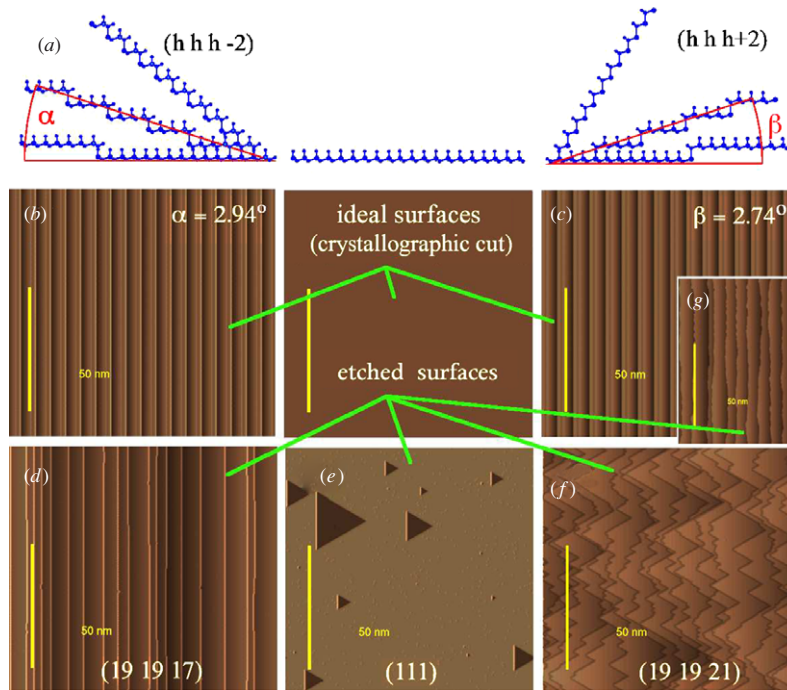
Figure 12. Different surface morphologies on miscut (1 1 1) at low concentration. Simulation.

Table 1. Low, mid and high concentration rates used for the simulations in figures 12, 14 and 15. The site types are TRI: trihydride; 2KSD: double kink from step dyhydride; KSD: single kink from step dihydride; SD: step dihydride, both horizontal (HSD) and vertical (VSD); TD: (1 0 0)-terrace dihydride; 2KSM: double-kink from step monohydride; KSM: single kink from step monohydride; SM: step monohydride; TM: terrace monohydride.

(n_1, n_2)	Low concentration	Etch rate Mid concentration	High concentrations	Site type
(1, >0)	1.0×10^0	1.0×10^0	1.0×10^0	TRI
(2, <4)	1.0×10^0	1.0×10^0	1.0×10^0	–
(2, 5)	$1.0 \times 10^0 / 1.0 \times 10^{-4a}$	$1.0 \times 10^0 / 1.0 \times 10^{-4a}$	$1.0 \times 10^0 / 1.0 \times 10^{-4a}$	2KSD
(2, 6)	1.0×10^{-1}	3.0×10^{-3}	1.0×10^{-4}	KSD
(2, 7)	1.0×10^{-2}	1.0×10^{-4}	1.0×10^{-6}	SD
(2, 8)	1.0×10^{-2}	1.0×10^{-4}	1.0×10^{-6}	TD
(2, >8)	0.0×10^0	0.0×10^0	0.0×10^0	–
(3, <5)	1.0×10^0	1.0×10^0	1.0×10^0	–
(3, 5)	1.0×10^0	$1.0 \times 10^0 / 1.0 \times 10^{-4a}$	$1.0 \times 10^0 / 1.0 \times 10^{-3a}$	2KSM
(3, 6)	1.0×10^{-4}	3.0×10^{-3}	1.0×10^{-1}	KSM
(3, 7)	1.0×10^{-6}	3.0×10^{-5}	1.0×10^{-3}	SM
(3, 8)	1.0×10^{-8}	1.0×10^{-8}	1.0×10^{-8}	–
(3, 9)	1.0×10^{-8}	1.0×10^{-8}	1.0×10^{-8}	TM
(3, >9)	0.0×10^0	0.0×10^0	0.0×10^0	–
(4, >0)	0.0×10^0	0.0×10^0	0.0×10^0	Bulk

a Values used for pinning.

It is important to recognize that double-kink stabilization does not necessarily occur only after the double-kink site has been already formed. Pinning of a double kink can be the result of a previous single-kink stabilization. In turn, this can result from a previously pinned step site. The three possibilities are outlined in figure 13. Due to the relative numbers of step, single-kink and double-kink sites on the surface and the differences between their life times we may argue that double-kink pinning is probably the result of step site stabilization. This, of course, eventually depends on the nature of the pinning agent and how it actually interacts with the different step and kink sites.

As noticed in section 1, the previous pinning phenomena are often referred to as *micromasking*, especially when discussing the dramatic effects of this microscopic mechanism on the morphology of the (1 0 0) and (1 1 0) surfaces. As pointed out above, a multitude of different agents such as hydrogen bubbles, polymerized residues, SiO_2 precipitates, semipermeable silicates and/or impurities might be at the root of micromasking.

At high concentration, the dependence of the morphology on misorientation from (1 1 1) has an opposite character to that at low concentration since the SD steps are stable and the SM are reactive. This is shown in figure 14, where the polygonal
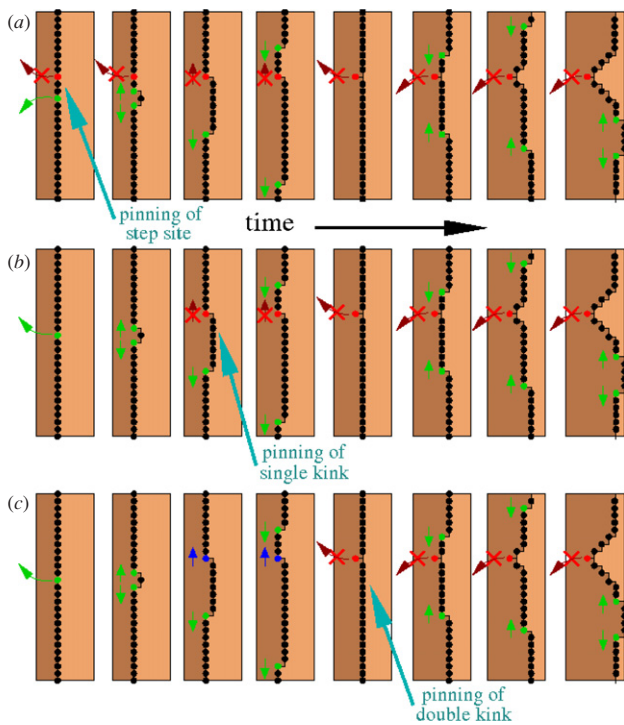
Figure 13. Schematic description of some convex tip pinning mechanisms on (1 1 1).

steps appear on the $(h\,h\,h-2)$ family and the straight steps on the $(h\,h\,h+2)$ family. As explained in section 2.2, the triangular pits on (1 1 1) are rotated 60° with respect to the orientation of similar pits at low concentration (figure 12). Exactly in the same way as it occurred at low concentration, the

polygonal steps require the existence of pinning or otherwise the steps become atomistically rough, as shown in figure 14(*g*).

At medium concentration, the steps can show 'spikes' in both misorientation families, depending on whether pinning occurs (figures 15(*g*)–(*i*)) or not (figures 15(*d*)–(*f*)).

In summary, in section 2 we have introduced the basic processes through which anisotropic etching takes place, namely, pit nucleation and step propagation, as well as the basic nomenclature for the surface sites and the major crystallographic features of the three main orientations. We also have described how the shape of the pits changes with concentration as a result of an underlying change in the relative reactivity of the SM and SD sites. We have presented the idea that the change in the relative reactivity of the two species might be the result of a selective blocking mechanism by the etchant cations. Finally, we have described the basic morphology of the stepped (1 1 1) surfaces which directly results from the underlying step propagation process. Polygonal and straight steps may appear depending on the concentration and the existence of micromasking.

3. Step bunching

Under most experimental conditions, the previous morphologies originating from the microscopic in origin step-flow process (assisted or not by pinning) on exact and misoriented (1 1 1) surfaces suffer modifications due to the existence of mesoscopic phenomena. Perhaps the most important of these effects is the formation of step bunches due to diffusion, as shown in figure 16. In this figure, the formation of polygonal steps is compared between experiment and simulation. Apart from the 100-fold difference in size scales, the largest difference between the two morphologies is the formation of step bunches in the experiment, an effect
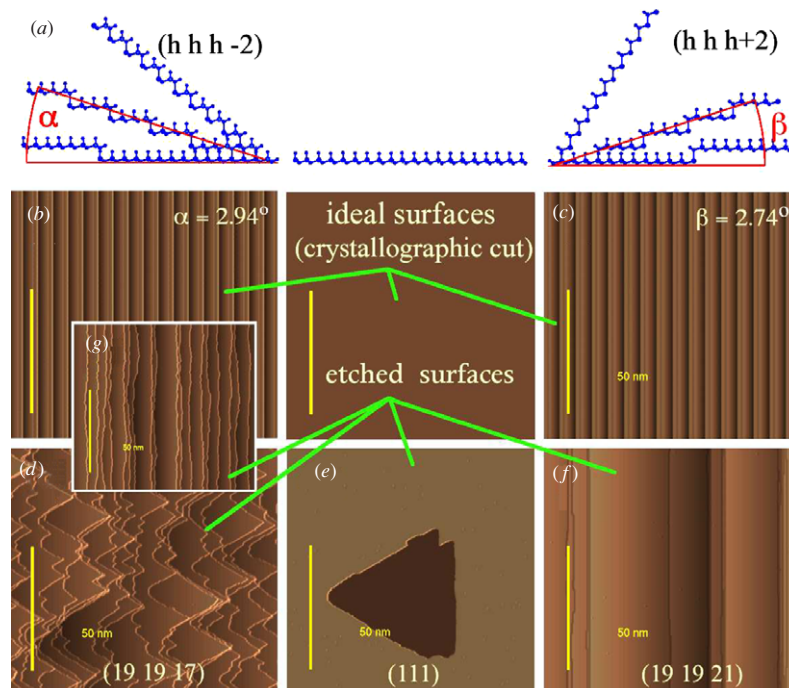
Figure 14. Different surface morphologies on miscut (1 1 1) at high concentration. Simulation.
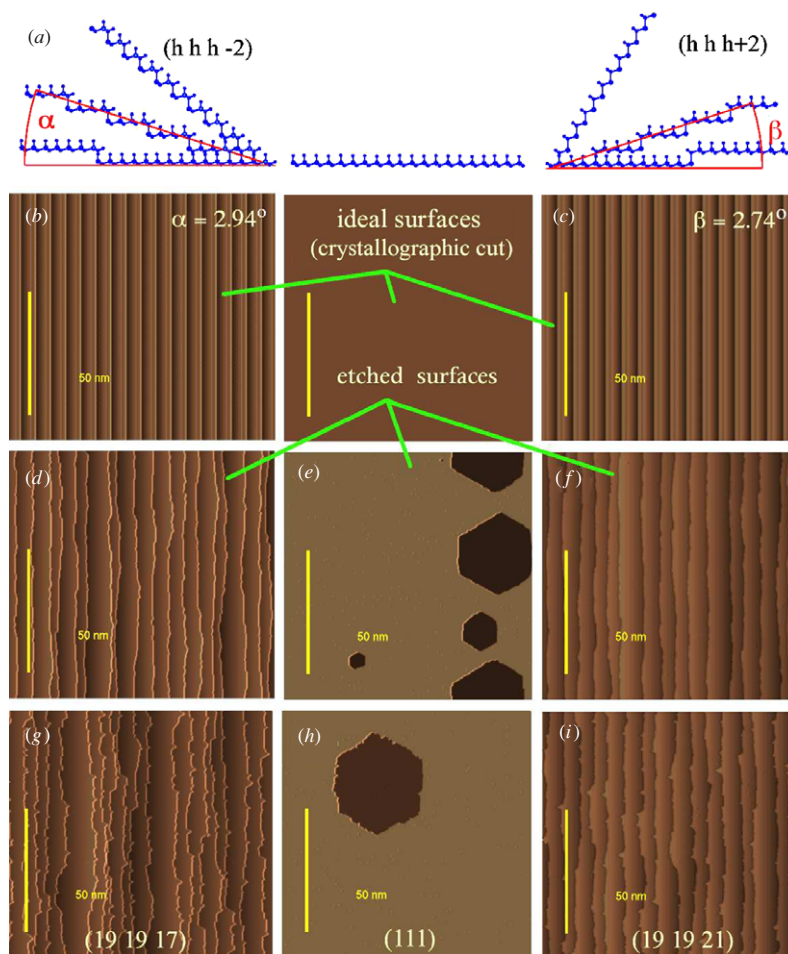
Figure 15. Different surface morphologies on misoriented (1 1 1) at medium concentration. Simulation.
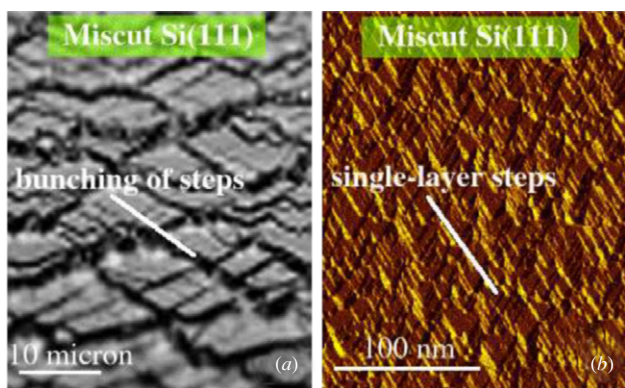
Figure 16. Step bunching on misaligned (1 1 1): (*a*) experiment (Sato Laboratory, Nagoya University, unpublished), (*b*) atomistic simulation.

that is not accounted for in the atomistic model used for the simulations. Similar step bunches are formed also on straight-stepped surfaces.

Step bunching is the result of a diffusion mechanism, where 'diffusion' refers to the transport of the reactants and/or products to/from the locations where they are consumed/produced. This diffusion transport typically takes a longer time than the atomistic reactions. As we

know, misaligned (1 1 1) surfaces are etched by preferentially unzipping the steps while the terrace sites remain very passive. Due to the transport delay and the localized consumption of the reactants at the steps, the etchant in contact with the surface develops inhomogenous regions in the proximity of the active regions, as sketched in figure 17. Although etchant depletion at the steps is characterized as local minima in the concentration profile (*c*), the inhomogeneities can also be associated with corresponding temperature gradients along the surface (*T*). The inhomogeneities are directly the result of a diffusion process which is lagging behind the high activity of certain regions on the surface.

A most important observation is that both the size and the magnitude of the etchant inhomogeneities will increase when two steps meet, something that can happen rather easily due to statistical fluctuations in the step-flow velocities. This will not only increase the size of the inhomogeneities but also the amount of etchant depletion and/or the magnitude of the temperature gradient in the resulting inhomogeneity. This is shown in figure 17(*b*) by drawing wider, higher variations in the temperature/concentration profiles. As an example, if a fluctuation brings two steps closer, the resulting pair will move more slowly (due to the larger etchant depletion) and it will be easier for a third step to catch up this pair. As the number of steps in the bunch grows, the bunch becomes even slower. Thus, the combined effect of fluctuations and the
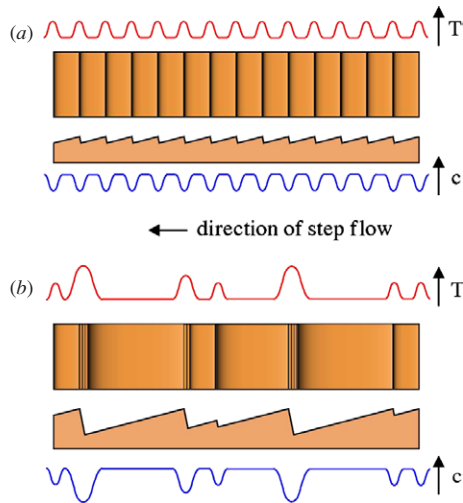
Figure 17. Step bunching on misaligned (1 1 1). Cartoon-like variations of the temperature (T) and concentration (c) are shown as examples of etchant inhomogeneities.

amplification of the etchant depletion in the inhomogeneity leads to the formation of the step bunches, where eventually tens, hundreds or even thousands of steps move together in concert. This description of the step-bunching process is due to Garcia *et al* [12, 13].

It is important to notice that in the same way as two steps may bunch together as the result of fluctuations in their propagation velocities, two steps belonging to a bunch may separate later on, thus splitting the bunch. In this way, the bunch size, understood as the number of steps bunched together, fluctuates about an average value determined by the etching conditions and the amount of steps per unit surface, determined by the surface misalignment.

In order to include diffusion in the kinetic Monte Carlo (KMC) simulations an incremental activity monitoring (IAM) has been recently proposed [29] as an alternative to the method presented by Garcia *et al* [13]. In one such simulation a surface atom i is given a removal rate k_i^0 whose value depends on the configuration of the neighborhood (e.g. on the number of first and second neighbors [9]) or on the type of site (see figure 6). Due to the diffusion phenomena, one expects a decrease in the removal rates at depletion regions and an increase if the reaction is strongly exothermic and the local rise in the temperature boosts the rates more than the etchant depletion damps them. This can be described by using a position and time-dependent diffusion factor D, such that $k_i = D k_i^0$ is the resultant removal rate. If $D = 1$, the etchant is in the homogenous state. $D < 1$ describes depletion inhomogeneities, resulting in a 'slow down' of the rates (or 'deceleration') and $D > 1$ describes an increase in the etch rate (i.e., 'boosting' or 'acceleration'). Since the formation of the inhomogeneities correlates with the activity on the surface, we assume that D is proportional to the normalized activity (ρ_A), as in $D = 1 + a\rho_A$. Here a is a parameter in the range $(-1, \infty)$ whose value determines whether D is equal to, greater than or smaller than 1. The normalized activity is defined as $\rho_A = A/\max(A)$, where the activity A is simply an integer variable which is incremented by one unit at the first and second neighbors of each removed atom. This provides a

way to record past removals. As more increments are added to A, a moving step leaves on A a track of its previous locations. The use of the diffusion factor D is inspired from [13], where it involves the density of steps instead of the normalized activity.

Recording the surface activity A is important because it enables sensing when and where two active regions overlap, increasing locally the normalized activity ρ_A and, with it, the diffusion factor D and the rates k_i. As a result, two active regions (which are typically two steps) can interact, effectively accelerating ($a > 0$) or decelerating ($a < 0$) their propagation. When a step pair propagates faster ($a > 0$), it eventually catches up a third step, further increasing the value of D. As more steps are involved, big step bunches are formed. If $a < 0$, D decreases when two steps come closer, thus slowing down the rates and making it possible for a third step to catch the pair, eventually also leading to step bunching.

Figure 18 shows typical time shots of the simulated surface morphology using the IAM method for stepped (1 1 1) surfaces with and without the diffusion effects at low concentration. The simulations show that step bunching develops as a result of the formation of inhomogenous regions in the etchant (figures 18(c)–(d)). In these simulations, A is truncated periodically every ΔT events in order to prevent an infinite memory of past events. This is done by finding the minimum value of $A(A_{min})$ and updating as $A = A - A_{min} - \Delta A$, where $\Delta A = 1$ ensures truncation even if $A_{min} = 0$. Additionally, the maximum of A is limited to a predefined value A_{max}. A fully detailed description of the IAM method including comparisons to other approaches is available in [29].

An interesting feature observed from figure 18(a) is that the polygonal steps can be formed without the participation of micromasking. As described in section 2.3, the formation of the polygonal steps can also be a result of local stabilization by pinning double-kink sites situated along the reactive steps (the SDs for low concentration), leading to the apparition of the opposite stable step family (the SMs at low concentration) delimiting the polygonal shapes. The formation of inhomogenous regions leads to a similar effect. For the case of figure 18(a), acceleration by the diffusion factor leads to the apparition of the stable steps by giving a larger boost to the sites away from the double-kink regions. A similar behavior is obtained for the case of deceleration (not shown) which gives a larger slow down to the double-kink regions.

In summary, this section has presented the formation of step bunches as a result of the delay between diffusion transport and the surface activity, typically concentrated at the steps. The delay leads to the formation of inhomogenous regions in the etchant. This diffusion effect is a key ingredient in order to understand the surface morphology during anisotropic etching.

4. Simplified etching model for (1 1 0) and (1 0 0)

Sections 2 and 3 have presented a model of anisotropic etching for exact and vicinal (1 1 1) orientations consisting primordially on a 'first-order' microscopic step-flow process with certain 'second-order' microscopic and mesoscopic corrections due to micromasking and diffusion. In the case of the exact and vicinal (1 1 0) and (1 0 0) surfaces, the 'corrections' to the step-flow model become imperative in order to describe the surface morphology.
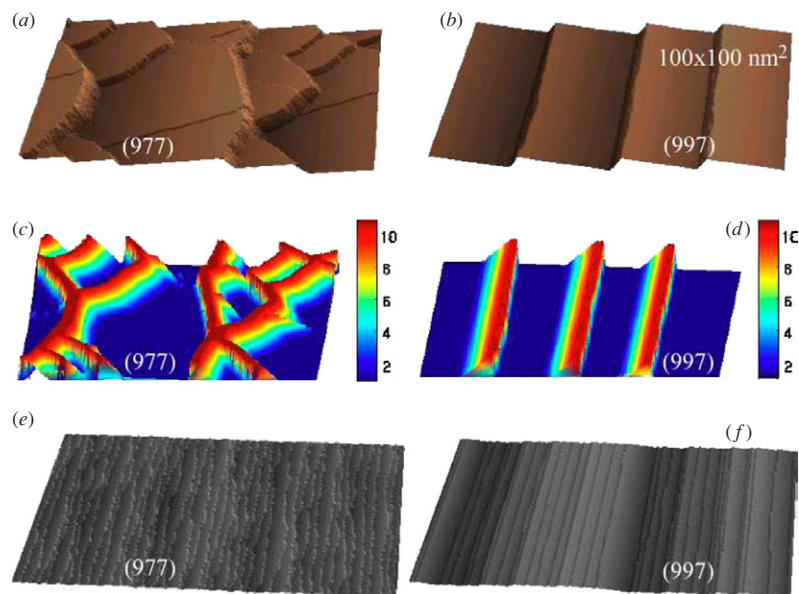
Figure 18. Examples of simulated $(h\,h\,h \pm 2)$ surfaces: $(a)-(b)$ morphologies showing bunching; $(c)-(d)$ diffusion factor for (a) and (b) showing the existence of inhomogeneities; $(e)-(f)$ morphologies without diffusion inhomogeneities. Step bunching in (a) through (d) generated using the IAM method ($a = 10.0$, $\Delta T = 0.4$, $A_{\max} = 18$, $\Delta A = 1$). No bunching in (e) and (f) obtained with $a = 0$. step-flow parameters as in column 2 of table 1 (low concentration).
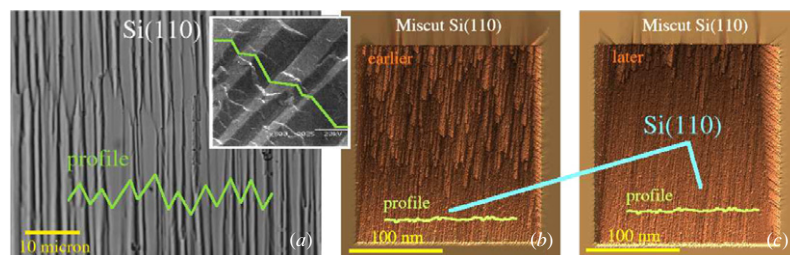
Figure 19. (a) Experimental zigzag structures on $(1\,1\,0)$ (large frame from figure 8 of [42] with permission from Elsevier; small frame from p 125 of [72]. (b), (c) Simulated morphology with a step-flow model that disregards step bunching and micromasking.

4.1. Simplified etching model for $(1\,1\,0)$

The etched surface morphology of $(1\,1\,0)$ is characterized by the appearance of the so-called *zigzag* structures, as shown in figure 19(a). The 'zigzag' terminology refers to the shape of the cross-section (or profile) of this morphology, as clarified by the insert in figure 19(a). In particular, it does not refer to other saw-shaped features that may be visible from a top view of the surface. The zigzag structures are characterized by displaying long stripes when viewed from the top, directly corresponding to the SM steps (see figure 8).

When one considers these elongated features and their zigzag cross-section together with the fact that the morphology of $(1\,1\,0)$ becomes macroscopically smooth when neither step bunching nor micromasking are considered in the simulations (see figure 19$(b)-(c)$), one may be inclined to believe that micromasking should have a leading role, pinning some sites along the SM steps and preventing the complete unzipping of the step, thus stabilizing the peaks of the zigzag structure [37, 54]. In principle, this is reasonable since, after all, the formation of the polygonal steps on miscut $(1\,1\,1)$ can be a consequence of micromasking, as shown in section 2.3. However, it has

been recently proposed that the zigzags are actually mainly a result of diffusion [29]. The idea is that the $(1\,1\,0)$ surface, which can be considered as a stepped $(1\,1\,1)$ surface, suffers step velocity fluctuations which lead to the formation of inhomogenous regions in the etchant and these inhomogeneities counter-affect the reaction rates of the steps, leading to the formation of the zigzags in a similar manner as the inhomogeneities cause step bunching on stepped $(1\,1\,1)$ surfaces.

The process is graphically explained in figure 20. As noticed in section 2 in the context of figure 8, $(1\,1\,0)$ is a limit example of a stepped $(1\,1\,1)$ surface without terraces. Thus, the ideal $(1\,1\,0)$ surface can be regarded as a large bunch of SM steps, as outlined in figures 20(a) and (b) for the two equivalent terrace families. From this perspective, the oversized bunch will necessarily split into smaller bunches during etching as a result of step velocity fluctuations, as outlined in figure 20(c), where the initial $(1\,1\,0)$ surface transforms into a collection of $(1\,1\,1)$ terraces separated by bunched SM steps. Considering larger systems, this behavior leads to a zigzag profile where each segment is in reality a collection of $(1\,1\,1)$ terraces separated by step bunches, as described in figures 20(d) and (e).
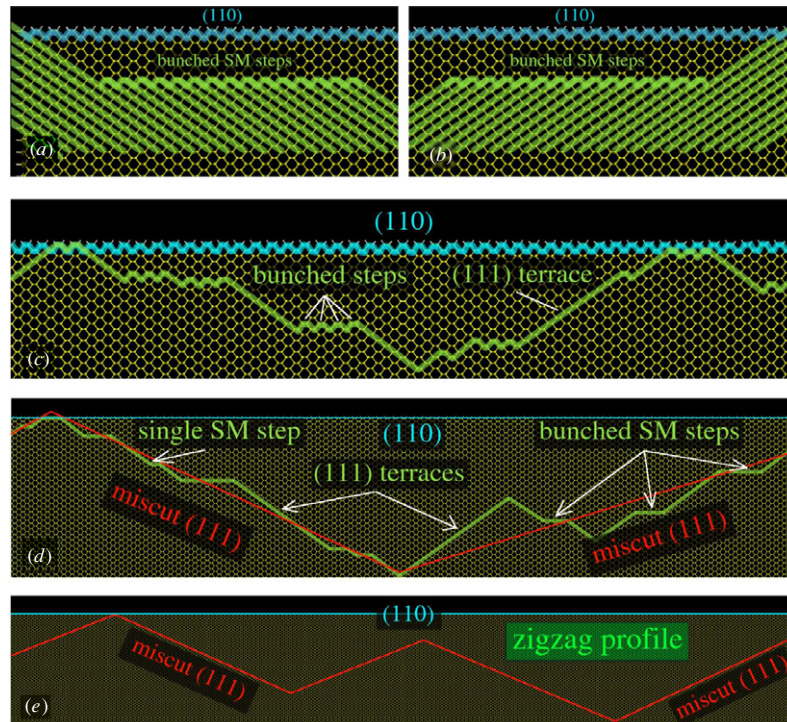
Figure 20. Schematic formation of a zigzag profile on (1 1 0) due to step bunching. From [29] (figure 11).
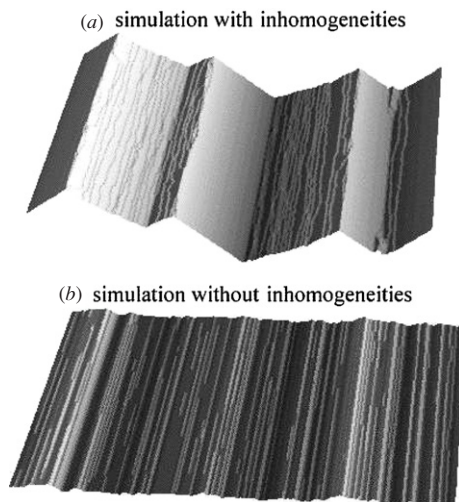
Figure 21. Formation of zigzag structures on (1 1 0). (*a*) Simulation using IAM ($a = 2.0$, $\Delta T = 1.4$, $A_{max} = 18$, $\Delta A = 1$). (*b*) Simulation without inhomogeneities ($a = 0$). System size is 100×100 nm^2. Compare to figure 19(*a*). From [29] (figure 12).

The formation of zigzags according to the previous process has been successfully simulated using the IAM method presented in section 3 [29]. As an example, figure 21 compares the formation of zigzag structures when etchant inhomogeneities are formed and the macroscopically flat morphology of (1 1 0) in the absence of the inhomogenous regions.

As the surface orientation is changed towards vicinal surfaces of (1 1 0), the long stripes characteristic of the zigzag structures necessarily break, forming the so-called *nosed-zigzags*, as shown in figure 22(*a*). The 'noses' are simply

induced by the misorientation [43], but their size is enlarged by step bunching. This is supported by the fact that the noses actually propagate along the surface in the direction of the SM steps, as outlined in figure 22(*c*). Since the noses of type A move up (which is the case for figure 22(*a*)), fluctuations in their velocities will lead to nose bunching. An interesting observation is that micromasking (presumably by metal impurities and/or etchant cations) can probably be the source of similar noses appearing on the exact (1 1 0) orientation, which are observed in some experiments, as demonstrated by figure 22(*b*). The fact that noses of type A, B and C appear on the surface of figure 22(*b*) indicates that the orientation is indeed exactly (1 1 0), in comparison to figure 22(*a*), where only type-A noses are formed due to the predominant role of misalignment. Of course, micromasking, if present, will increase the number of noses also on the vicinal surfaces.

The specific role of diffusion and micromasking in the formation of the nosed zigzag profiles needs to be further clarified by means of simulations that will consider their combined effects. As mentioned in section 1, some metal impurities (especially Cu) and the etchant cations may selectively block the step, single-kink and/or double-kink sites, becoming an important source of pinning.

The previous description of the zigzag structures applies to the surface morphology of exact and vicinal (1 1 0) at low concentration, where the SM steps are stable. At high concentration, these steps are more reactive than the SD steps, as we learned in section 2.2. As a result, the surface morphology changes quite dramatically, especially if micromasking is present. We will return to this in section 4.3, after considering a similar issue that occurs on (1 0 0) at low concentration.
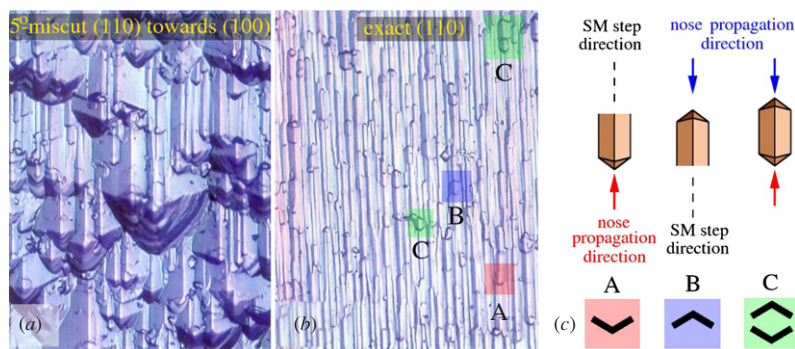
Figure 22. Nosed zigzag structures on vicinal and exact (1 1 0). Experimental images (*a*), (*b*) from Sato Laboratory, Nagoya University (unpublished).
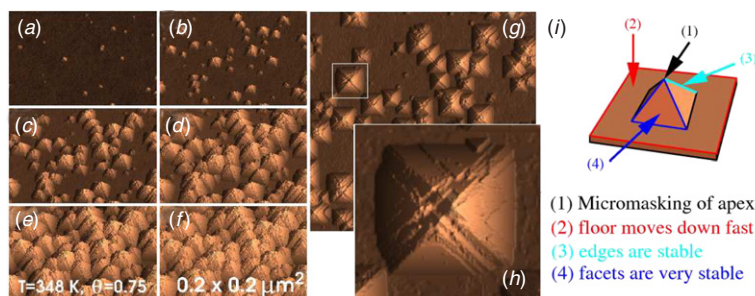
Figure 23. Simulated pyramidal hillocks on (1 0 0). (*a*)–(*f*) Snapshots at increasing times during a simulation. (*g*) top view of (*c*). (*h*) Detail from (*g*). (*i*) The four necessary conditions for hillock formation. (*a*)–(*h*) from [43] (figure 2).
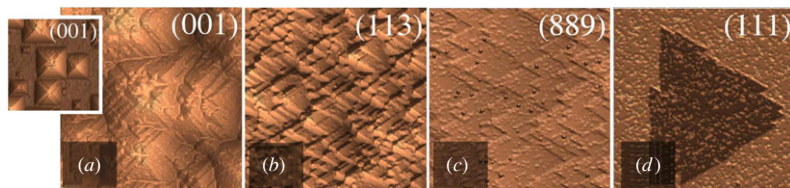
Figure 24. Relation between pyramidal hillocks on (1 0 0) and polygonal steps on (*h h h* + 2). (From simulations.) This figure contains frames from figure 14 of [43].

In summary, this section has presented the idea that the zigzag structures characteristic of the etched morphology of (1 1 0) are mainly the result of diffusion inhomogeneities. According to the presented description, it is improbable that micromasking is the origin of these structures. However, micromasking can be singled out as the one mechanism responsible for the formation of the zigzag noses on exactly oriented (1 1 0) surfaces and the amplification of the nose sizes on miscut (1 1 0).

4.2. Simplified etching model for (1 0 0)

As in the case of (1 1 0), the surface morphology of (1 0 0) is dominated by the 'corrections' to the step-flow model of (1 1 1), namely, micromasking and diffusion. At low concentration, the most characteristic feature of this surface is the formation of pyramidal hillocks [31, 32, 34, 36, 38, 70]. An example of this morphology is shown in figure 23. At low magnification, the hillocks appear as regular pentahedra composed of four lateral (1 1 1) crystallographic planes on the (1 0 0) base plane, as depicted in figure 23(*i*). Under

closer examination, the hillocks reveal a more complicated morphology. Typically, the apex is not a unique point and, the edges and facets display different levels of roughness, as the detail in figure 23(*h*) shows. Depending on conditions, the hillocks may completely cover the surface after a long etching time [34], as shown in figure 23(*f*). If this occurs, the surface is said to be completely *texturized* [71].

Hillock formation is a process that requires four conditions to be satisfied simultaneously [38, 43], as indicated in figure 23(*i*): (1) the existence of a micromasking agent which stabilizes the apex atom/s; (2) a fast downward motion of the floor surface; (3) stable pyramidal edges; and (4) very stable pyramidal facets. Since the (1 0 0) surface may be considered as a SD stepped (1 1 1) surface without terraces (section 2.1), the formation of the hillocks can be regarded as the limiting case of the formation of polygonal steps on the (*h h h* + 2) family of (1 1 1) miscuts, a process due to double-kink pinning (section 2.3), although it can also be due to diffusion (section 3). This is graphically demonstrated in figure 24. Note that figure 24(*a*) is a fully texturized (1 0 0) surface (i.e., completely covered by hillocks). It corresponds to a later time than the small insert shown in it.
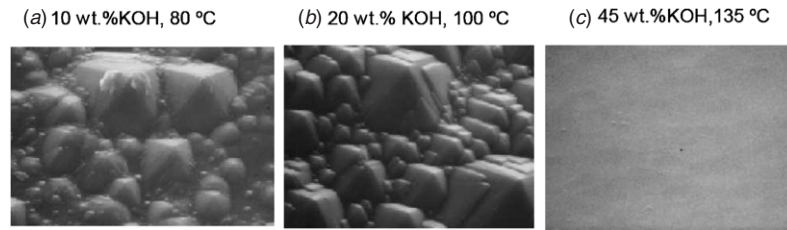
Figure 25. (1 0 0) morphology dependence on concentration. From [72] (p 21).
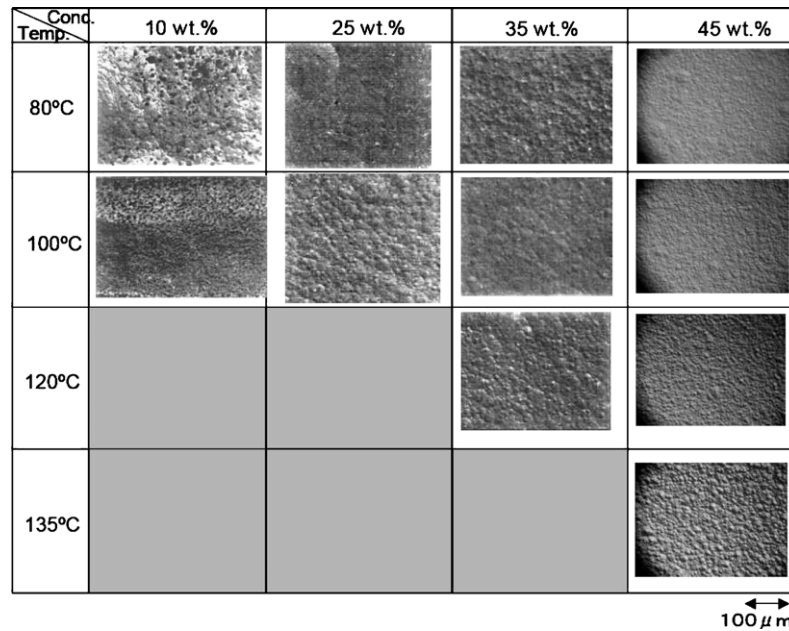
Figure 26. Morphology of (1 0 0) as a function of KOH concentration and temperature. Optical differential interference contrast. From [72] (p 20).

It is very important to realize that all four conditions in figure 23(*i*) are necessary. If any one of them fails, the hillocks will not be formed. For instance, if there is no pinning, the hillocks cannot be generated, even if the other three conditions are fully satisfied. Similarly, the pyramids cannot be formed if the atoms at the pyramid edges are very reactive, even under strong micromasking and compliance with the other two conditions. This last case is of particular interest, since the pyramid edges correspond to SM steps (as graphically demonstrated by figure 24) and precisely these steps are known to become reactive at high concentrations. Thus, it is easy to understand why hillocks are not formed on (1 0 0) at high concentrations even in the presence of micromasks, as shown in figure 25. Additionally in this case, the SD steps (which control the downward motion of the bottom floor) become themselves rather stable when increasing the concentration, which leads also to the failure of the second condition.

Concerning the generation of the pyramidal hillocks, the formation of inhomogeneities seems to have a reduced impact on the overall process. Although section 3 has shown that the polygonal steps can develop as a result of inhomogeneities, our simulations show that the hillocks do not appear by only diffusion effects. They need an atomic scale micromasking agent. We cannot rule out that inhomogeneity formation may

effectively amplify the size of the hillocks, in a similar manner as the hydrogen bubbles. See [43] for an overview of the role of hydrogen and other agents in micromasking.

Nevertheless, diffusion can dramatically affect the surface morphology of (1 0 0) in the absence of micromasking. In this case, typically the morphology of this surface resembles that of an orange skin, full of round pits, as shown in figure 26. Note that this figure has been obtained using optical differential interference microscopy, which enables the observation of shallow features such as the floor surface instead of the hillocks. This feature can be easily understood by comparing the lower-right frame of figure 26 with figure 25(*c*) or the black square spots in the upper-left frame of figure 26 with the hillocks in figure 25(*a*). Figure 26 shows that the morphology of the floor surface consists of numerous round pits at both low and high concentration and that the presence or absence of the hillocks is irrelevant for the pits.

The circular shape of the pits can be understood from the original step-flow process. As shown by figure 27, if micromasking is switched off in a simulation that uses only a simple step-flow model with no diffusion effects (as previously in section 2.3), the four-fold symmetry of the (1 0 0) surface leads to shallow square pits which become round features as the steps propagate in the two perpendicular, in-plane directions. Although the shallow features are far
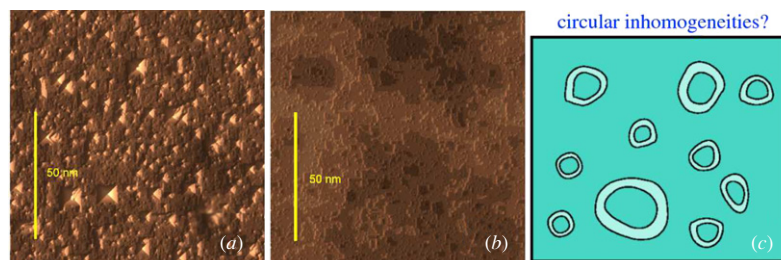
Figure 27. Simulated morphology of (1 0 0) with (*a*) and without micromasking (*b*). (*c*) Proposed shape of the etchant inhomogeneities on (1 0 0).

from the round pits observed experimentally, it is easy to understand how the two-layer-deep square pits transform into circular shapes as more layers are involved. As suggested by figure 27(*c*), the local variations in the etchant concentration and/or temperature will have the shape of circular rings, simply because the steps have a tendency to become round from the original square shape. Also because a square shape cannot survive for long in a fluid. The formation of *doughnut*-shaped inhomogeneities is probably a key ingredient for generating larger and deeper round pits. This is very similar to the way in which the long, thin, sausage-like inhomogeneities on (1 1 0) lead to long, deep zigzag structures. The only difference between the doughnut- and sausage-shaped inhomogeneities is the difference in their spacial symmetry, which follows that of the underlying surfaces: (1 1 0) has two-fold symmetry and leads to elongated features; (1 0 0) has four-fold symmetry and leads to (rounded) square features.

In the future, it will be exciting to see whether simulations using the IAM method of section 3 can show if the formation of doughnut-shaped inhomogeneities leads or not to the development of shallow round pits.

To sum up this section, we have presented an overview of the etched morphology of (1 0 0), characterized by pyramidal hillocks at low concentration and shallow round pits at high. The hillocks appear as a consequence of micromasking as well as due to favorable conditions of relative stability of the edges, high stability of the facets and high reactivity of the bottom floor surface. At high concentration the relative stability of the different sites is changed and the pyramid formation is disabled. Diffusion is considered to have a minor role in the generation of the hillocks, although it may help to amplify their size. In opposition, the round pits, which are formed at low and high concentration, are proposed to be due to diffusion and to follow the formation of circular inhomogeneities in the etchant, just in the same manner and for the same reason as the zigzag structures are formed on (1 1 0).

4.3. Back to (1 1 0): formation of hillocks at high concentration

As described in section 4.1, (1 1 0) displays zigzag structures at low concentration, a phenomenon that can be described by using a microscopic step-flow model modified by including step bunching and micromasking. A major element in this description is the stability of the SM steps. However, as the concentration is increased, the SM steps become more reactive

and the long zigzag structures fail to be formed as condition (3) is violated. Interestingly, the increase in the reactivity of the SM steps is accompanied by a stabilization of the SD steps, a situation which enables the formation of hillock structures provided that also micromasking is satisfied. This change of morphology is shown in figure 28. The characteristic zigzags at 10–35 wt% KOH are replaced by hillocks at 45 wt%. In this particular case, the hillocks have grown so large that they interact with each other, producing a completely texturized surface.

Figure 29 shows typical hillocks on a non-texturized (1 1 0) surface. These hillocks are different from those appearing on (1 0 0) at low concentration. Not only they appear on different surface orientations and at different concentrations, but also the crystallographic orientation of the facets is different. For (1 0 0) they correspond to (1 1 1). For (1 1 0) the facets are stepped surfaces of type (h h h+2), such as (1 1 3), the particular orientation being dependent on the actual experimental conditions. Besides, the base of the pyramidal hillocks on (1 0 0) is square whilst it is trapezoidal for the hillocks on (1 1 0). As a result, the projection of two of the edges of the trapezoidal hillocks onto the floor surface aligns with the direction of the SM steps and the projection of the other two is perpendicular, as illustrated in figure 29(*d*).

As shown in figure 30 the idealized shape of the trapezoidal hillocks (figure 30(*b*)) can be understood by comparing it with other features, such as a rectangular hillock (figure 30(*a*)) and a prism (figure 30(*c*)). To illustrate this point, a description of the three shapes is given in figures 30(*d*)–(*f*) using (1 1 1) planes. The difference between the three shapes is the relative number of terrace, step and double-kink sites.

In the rectangular hillock the stability of the SD steps is comparable to that of the terrace sites, an unrealistic assumption that explains why these hillocks are not observed. In the case of the prism, it is the SM steps that are stable, not the SD steps. This corresponds to the zigzag structures observed at low concentration. It is only in the trapezoidal hillocks that the SD steps are both more reactive than the terraces and more stable than the SM steps, which is the case at high concentration. This is consistent with the fact that the trapezoidal hillock of figure 30(*e*) can be considered as the result of propagating the SD steps of the rectangular hillock in figure 30(*d*). Depending on the actual relative stability of the terrace and the SD step sites, the crystallographic orientation of the facets will change.

As in the case of the pyramidal hillocks observed on (1 0 0) at low concentration, micromasking is an essential

Conc. Temp.	10 wt.%	25 wt.%	35 wt.%	45 wt.%
80°C				
100°C				
120°C				
135°C				

100 μm
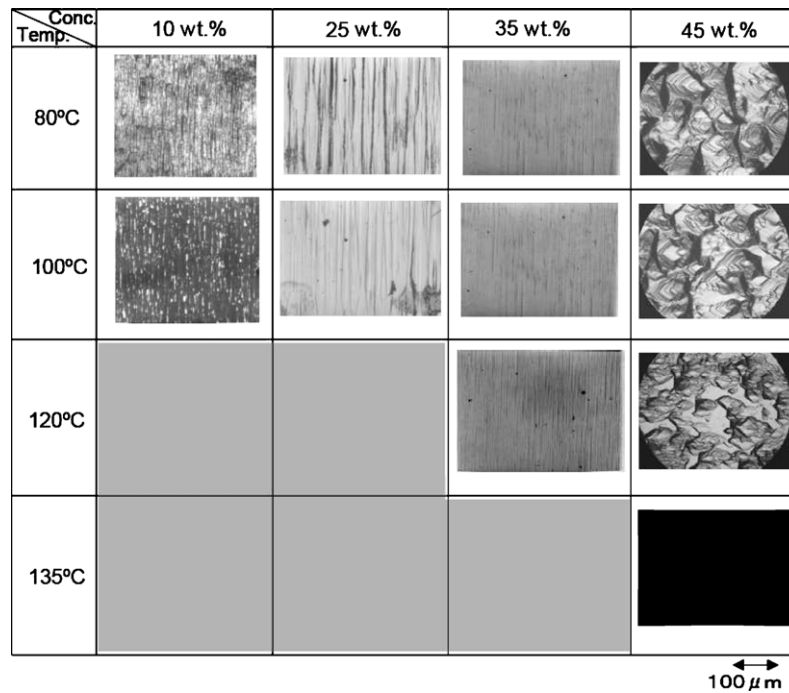
Figure 28. Morphology of (1 1 0) as a function of KOH concentration and temperature. From [72] (p 23).
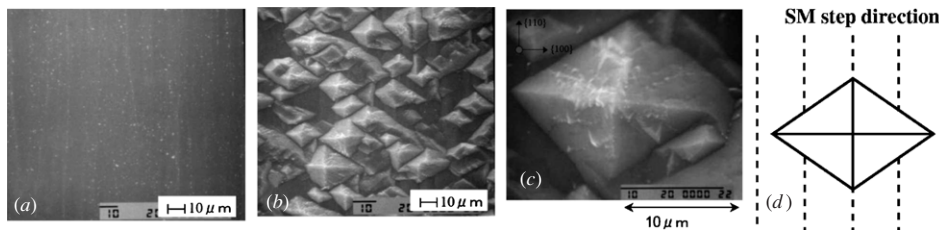
Figure 29. (*a*), (*b*) Comparison of the (1 1 0) morphology with and without hillocks. (*c*) Detail of a hillock in (*b*). 32 wt% KOH, 110 C. (*d*) Projection of the idealized hillock shape on the floor surface. For (*a*) Cu content is 21 ppb. For (*b*) and (*c*) Cu content is 360 ppb. From [72] .
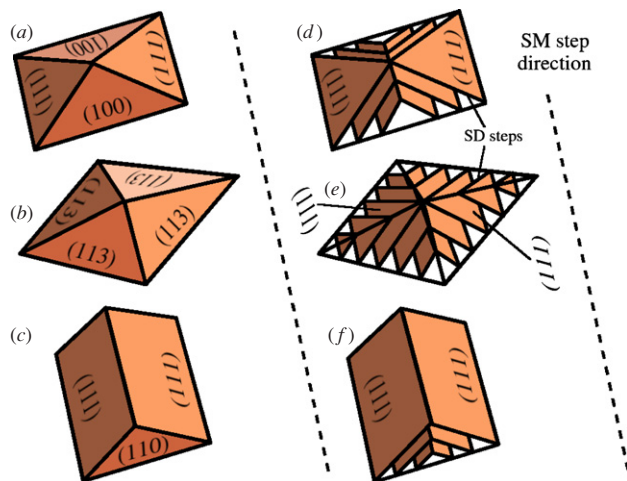
Figure 30. (*a*)–(*c*) Schematic potential shapes for morphology features on (1 1 0). (*d*)–(*f*) Description of the shapes using (1 1 1) terraces.

prerequisite for the formation of the trapezoidal hillocks on (1 1 0). As an example, figure 30(*e*) shows that the two edges

whose projection is perpendicular to the SM step direction are composed of pinned SM double kinks, which form the tips of the triangular (1 1 1) planes shown in that figure. This is similar to the pinning of SM double kinks in figure 14 leading to SD delimited polygonal steps at high concentration. Thus, it is necessary to understand better how different micromasking agents can affect the reactivity of these and other sites.

As in the case of the pyramidal hillocks on (1 0 0), we may argue that inhomogeneity formation due to diffusion will have a small role in shaping the trapezoidal hillocks, although it may be important as a mechanism for hillock size amplification.

As a summary for section 4 we conclude that the basic morphology of (1 1 0) and (1 0 0), namely that of zigzags for (1 1 0) and round pits for (1 0 0), results from the formation of inhomogenous regions in the etchant. The different shape of the inhomogeneities is mostly determined by the underlying crystallographic symmetry of two surfaces. On top of these basic morphologies, superimposed hillocks can be generated on both surfaces as a result of micromasking. In accordance with four rules identified for the stability of the hillocks, the defects can only be generated at low concentration for (1 0 0) and at high concentration for (1 1 0).
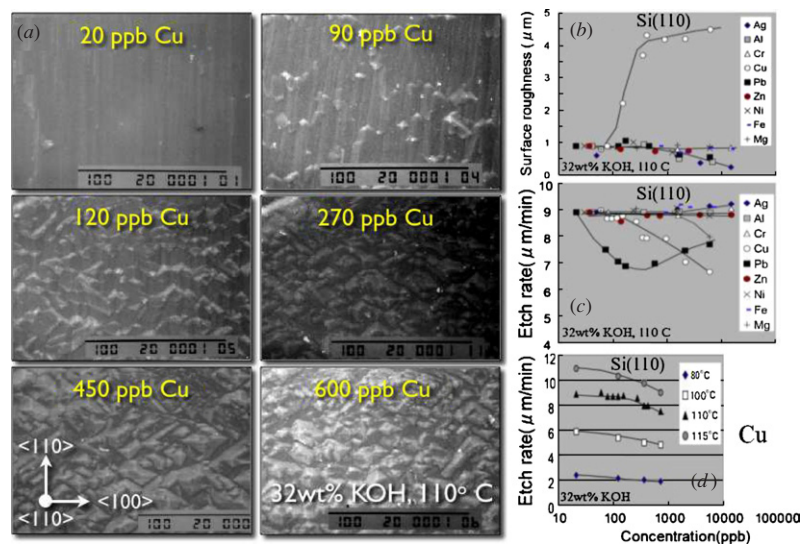
Figure 31. Effect of the addition of metal impurities on (*a*) the morphology, (*b*) the surface roughness and (*c*), (*d*) the etch rate of Si(1 1 0). From [72] (pp 36, 38, 39, 44).

5. Micromasking by metal impurities

As we have seen in section 4, micromasking can have dramatic effects on the surface morphology of both (1 0 0) and (1 1 0). In this section, we use the simplified etching model based on step-flow, micromasking and diffusion in order to explain the changes observed experimentally in the morphologic features and the etch rate due to the presence and/or addition of a number of metal impurities such as Ag, Al, Cr, Cu, Pb, Zn, Ni, Fe and Mg to the etchant.

Figure 31 shows the effect of the addition of small amounts of these metals in the etching bath. According to these experimental results, Cu has the most prominent effect among all impurities, affecting both the surface roughness and the etch rate of (1 1 0). All other impurities seem to have no effect, except for Pb, which clearly results into a lower etch rate, although it has a vanishing effect on the roughness. By comparing figures 31(*a*) and (*b*), the increase in the surface roughness due to the addition of Cu can be simply understood as the result of the formation of trapezoidal hillocks. Since the hillock density increases with the Cu content, it becomes apparent that the Cu impurities probably act as micromasks.

Note that the formation of the hillocks results into a larger number of SD steps (in the hillock facets), eventually dominating in number over the faster SM steps. This explains the reduction in etch rate observed in figure 31(*c*). Similar etch rate reductions occur due to the addition of Cu at other temperatures according to figure 31(*d*), suggesting that the trapezoidal hillocks are formed due to micromasking at all temperatures within this range.

As figure 32 shows, the addition of Cu also affects the surface morphology of (1 0 0), although it does not affect the etch rate. According to these measurements, (1 0 0) is typically ten times smoother than (1 1 0). Comparison of figure 32(*a*) and (*b*) explains the increase in the surface roughness as due to the formation of deeper round pits. This change in morphology can be compared to that occurring between figures 19(*a*) and 22(*b*) for (1 1 0), where the formation of noses in the latter

is due to micromasking. In the same manner, micromasking along the circular steps on (1 0 0) pins the surface at certain locations, resulting in deeper features whose shape can be accentuated by diffusion phenomena. Since the SD steps are more stable than the SM steps at this concentration (as supported by the fact that the etch rate of (1 0 0) is lower than that of (1 1 0)), the pyramidal hillocks characteristic of this surface at lower concentrations cannot be formed. Because the hillocks cannot appear, no significant reduction in the etch rate is expected. This is in agreement with figure 32(*d*), where the etch rate decreases only slightly or stays constant.

As for (1 1 0), the other metal impurities have no appreciable effect on (1 0 0), except for Pb, which affects the etch rate but not the surface morphology, in just the same manner as described for (1 1 0).

The previous experimental results concern a medium concentration of KOH, namely 32 wt%. Figure 33 shows the effect of the addition of Cu on the surface morphology of (1 1 0) and (1 0 0) at other concentrations. At the lowest concentration (10 wt%) before the addition of Cu, (1 1 0) exhibits the typical long zigzag structures. These structures become less prominent as the concentration is increased. When Cu is added, many noses are induced at 10 wt%, eventually being transformed into trapezoidal hillocks at 32 wt%. This is due to the underlying change in the stability of the SD and SM steps with concentration.

For (1 0 0), the addition of Cu at 10 wt% results in a larger amount of larger pyramidal hillocks, stressing again the micromasking role by Cu. At 15 wt%, the number of hillocks overwhelmingly increases due to the addition of the impurities, although the hillock size clearly decreases. This corresponds to a situation where there is an increased amount of micromasking but a reduced stability in the pyramidal edges, in agreement with the fact that the reactivity of the SM steps increases with concentration. Eventually, the number of hillocks decreases with increasing concentration due to the change in the stability of the SD and SM steps, as shown for 22 and 32 wt% KOH.
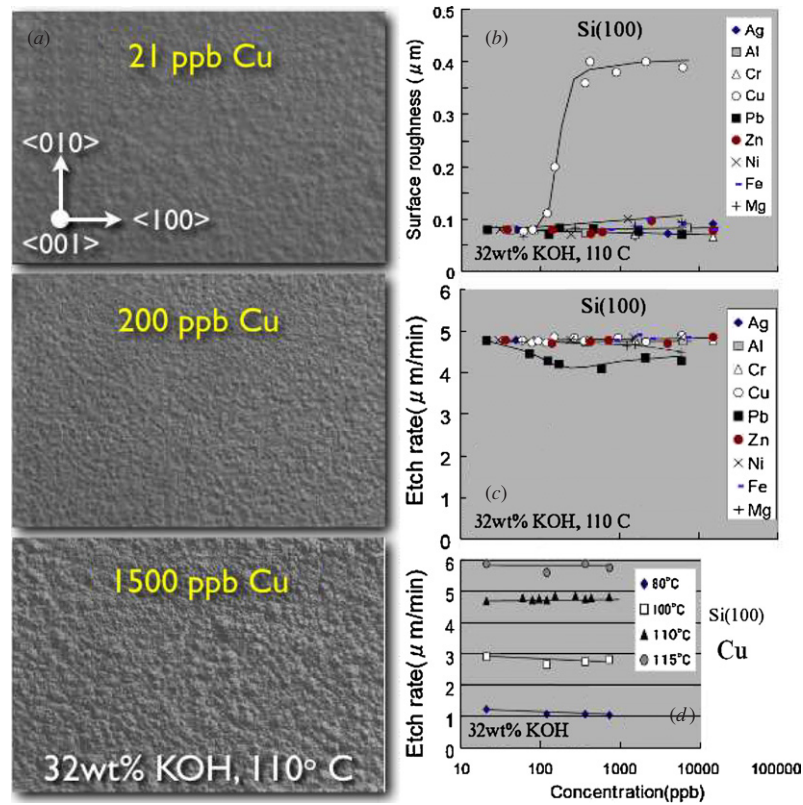
Figure 32. Effect of the addition of metal impurities on (*a*) the morphology, (*b*) the surface roughness and (*c*), (*d*) the etch rate of Si(1 0 0). From [72] p 36, 38, 39, 42.
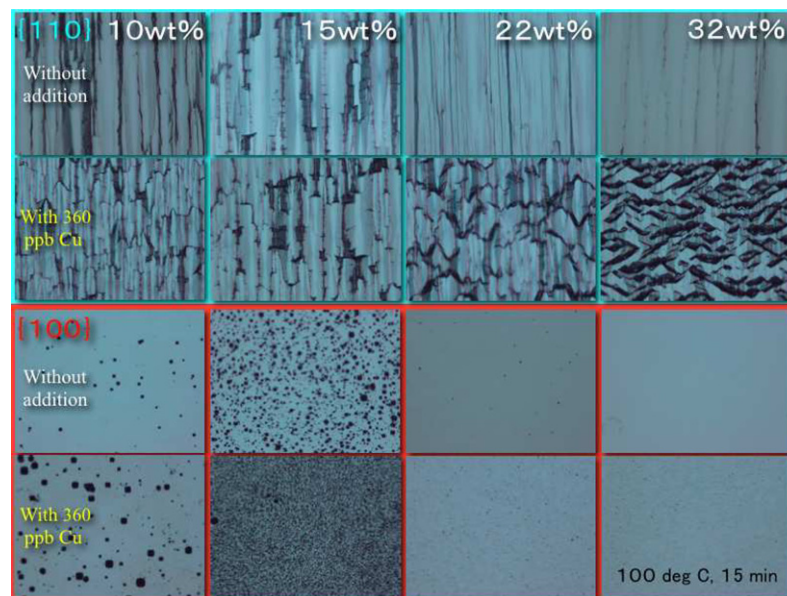
Figure 33. Effect of Cu impurities on the surface morphology at different concentrations. Denso Corp. unpublished.

The previous figures have shown that Cu can have a dramatic impact on the etch rate and, the surface morphology and roughness of both (1 1 0) and (1 0 0). As compared to other metal impurities, Cu seems to have a particular preference to adsorb on the Si surface. We are currently determining the adsorption energies of Cu and other metals at different surface sites using first principles calculations with the ultimate purpose of using these values in kinetic Monte Carlo simulations. According to preliminary results, Cu and Pb adsorb to the surface while Mg does not, in agreement with the previous experiments. At low concentration, Cu adsorption is more selective, occurring preferentially at the dihydride steps and the kinks of both the monohydride and dihydride steps. At high concentration, adsorption is less selective. In
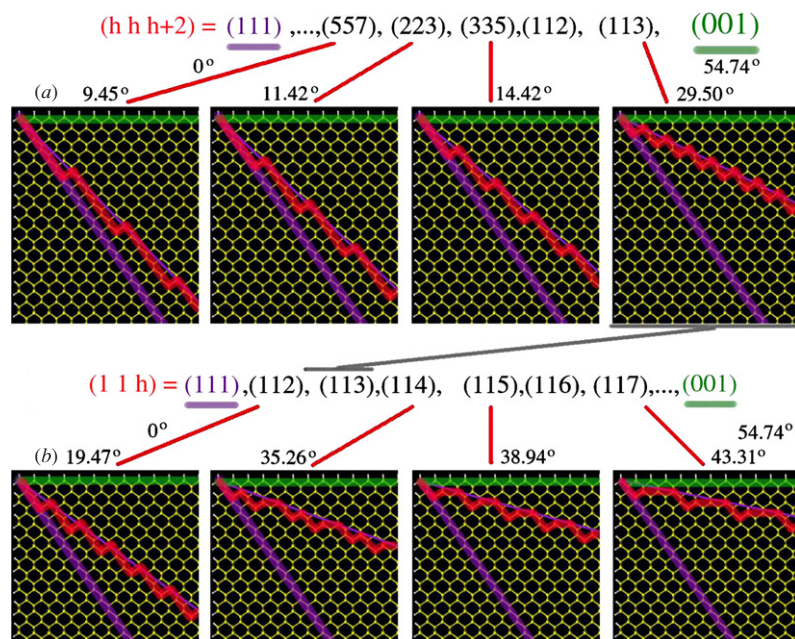
Figure 34. Crystallographic profile of the stepped surfaces between (1 1 1) and (1 0 0).

general terms, this agrees well with the experimental results, explaining why Cu can act as a micromask creating hillocks both on (1 0 0) and (1 1 0). The full details of the study will be reported later.

6. Other orientations

Sections 2 through 4 have presented a simplified etching model for the three principal orientations based on the propagation of steps modified by including diffusion effects and micromasking as the key ingredients to explain the different morphologies. In principle, the model can also be used to understand the behavior of other orientations. In particular, we are specially interested in (1 1 3) and (133) since they are often—although not always—found to be the fastest etching orientations.

As illustrated in figure 34(*a*), (1 1 3) can be regarded as a special orientation because it is the last representative of the (*h h h* + 2) family of (1 1 1) stepped surfaces before reaching the final (0 0 1). In this series, the surface (*h h h*+2) has exactly *h* TM sites per terrace. As an example, careful inspection of the figure shows that (557) has five TMs in each terrace, (446) has four, (335) has three, etc. Note that (446) becomes (223) after correction by the common divisor 2. In this respect, (1 1 3) has the lowest density of terrace sites in the whole series, if one disregards (0 0 1). Since a larger number of terraces will result into a slower etch rate, (1 1 3) will be the fastest orientation of this series, except maybe when compared to (0 0 1).

There is another family of surfaces that continues approaching (0 0 1) where (1 1 3) finishes: the (11*h*) family, as shown in figure 34(*b*). As *h* increases, the (11*h*) surfaces progressively display a larger number of SD step sites per terrace. The SD/TM ratio is actually calculated as (*h* − 1)/2. As an example, (1 1 2) has 0.5 step sites per terrace site, (1 1 3)

has 1, (1 1 4) 1.5, (1 1 5) 2 and so on. As an inspection of figure 34(*b*) shows, all the surfaces with SD/TM ratio larger than 1 show step bunching already in the ideal crystallographic cut. Thus, we may argue that diffusion effects are more significant for the (11*h*) family than for the (*h h h* + 2) family. In particular, we may expect that (0 0 1) will be the most strongly affected orientation by diffusion, especially at low concentration, as the SD steps contain the most active sites. The effect should then gradually decay as we move towards (1 1 1) in the (11*h*) family.

The previous conclusion is based on the fact that the formation of the etchant depletion regions (or inhomogeneities) is more probable on the regions where there is larger reactivity. In this way, if diffusion slows down the overall etch rate due to etchant depletion, the more active a surface is, the more it will be slowed down due to diffusion.

The previous crystallographic insight into the (*h h h* + 2) and (11*h*) surface families allows us to qualitatively explain why the etch rate typically experiences a maximum at (1 1 3) (or close to it) at low concentration. According to figure 35(*a*), the etch rate of the different miscut surfaces varies as $r = v \sin \theta$ when considering a simple step-flow model where v is the step propagation velocity. This familiar curve is shown in figure 35(*b*). If we assume that the bunch step velocity V varies as $\cos^2 \theta$ in an attempt to describe the slow down that diffusion produces especially in the (11*h*) family, the overall etch rate R of the bunched surfaces then varies as $R \sim \sin \theta \cos^2 \theta$, which displays a maximum at an intermediate orientation, as shown in figure 35(*b*). This qualitatively explains how diffusion may slow down the fastest orientation of a microscopic step-flow model, shifting the maximum towards a stepped surface such as (1 1 3) (the fastest surface in the (*h h h* + 2) family), where diffusion has a less dramatic effect.

If the previous explanation of the etch rate maximum at (1 1 3) (or close to it) due to diffusion is true, it should be

$$r = \frac{\delta z}{\delta t} = v \sin\phi$$

$$R = V \sin\phi$$

$$V \sim \cos^2(\phi)$$

$$\delta t = \frac{1}{v}$$

$$\delta z = h \cos\phi$$

$$\frac{h}{l} = \tan\phi$$

(a)

step flow ~ sin(Φ)

step flow x diffusion

diffusion ~ cos²(Φ)

(111)   (001)

(b)
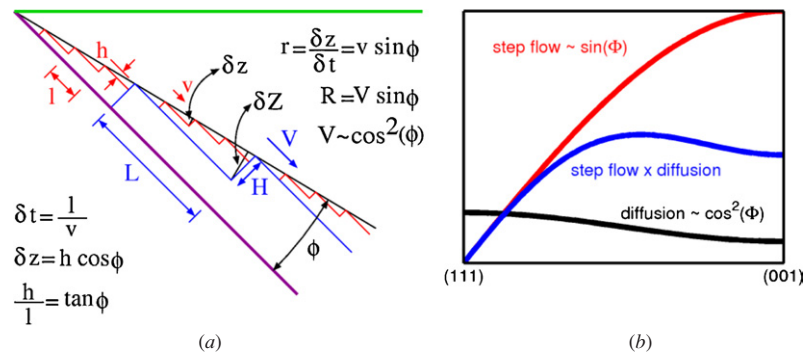
Figure 35. (a) Etch rate for a simple step-flow model with (R) and without (r) step bunching. (b) Effect of step bunching on the etch rate.

80°C with agitation   80.0°C without agitation
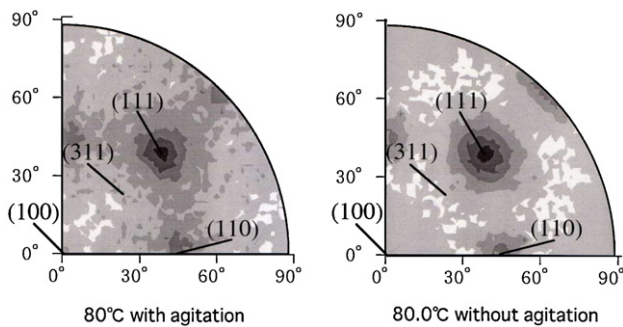
Figure 36. Stereographic projection of the etch rate showing the shift in the etch rate maximum due to stirring in 10 vol%TMAH. Sato Laboratory.

possible to restore the maximum at (1 0 0) by avoiding the formation of inhomogeneities, which can be done by stirring. Figure 36 shows that the maximum etch rate shifts indeed towards (1 0 0) when agitating the etchant. The magnitude of the shift should depend on the stirring power, which explains

why the maximum has not been completely restored into (1 0 0). Typically, the etch rate in TMAH is lower than in KOH. The difference in the activity of the two etchants explains why moderate stirring does not generally affect the position of the maximum in KOH. Presumably, stronger agitation should result in a similar effect as observed for TMAH.

At high concentration, the SD steps become stable. This decrease in activity will lead to less, softer inhomogeneities. As a result, the diffusion effects become less critical and, as the concentration is increased, the maximum etch rate between (1 1 1) and (1 0 0) gradually shifts towards (1 0 0).

If we turn now our attention to the surfaces which lie between (1 1 1) and (1 1 0), it is easy to predict that there are also two surface families, namely, the $(h\,h\,h-2)$ and the $(h\,h\,1)$ surfaces, whose ideal crystallographic cuts display SM steps (see figure 37). Now the special role is played by (3 3 1). Since the SM sites are the most reactive at high concentration but they are rather stable at low concentration, the diffusion effects are expected to affect the position of the etch rate only at high concentration, in a similar manner as they affect the SD-stepped surfaces at low concentration. Thus, figure 38

$(h\,h\,h\text{-}2) = (111),...,(775),(332),(553),(221),(331),(110)$

$(h\,h\,1) = (111),(221)\quad,(331),(441),\ (551),(661),\ (771),...,(110)$
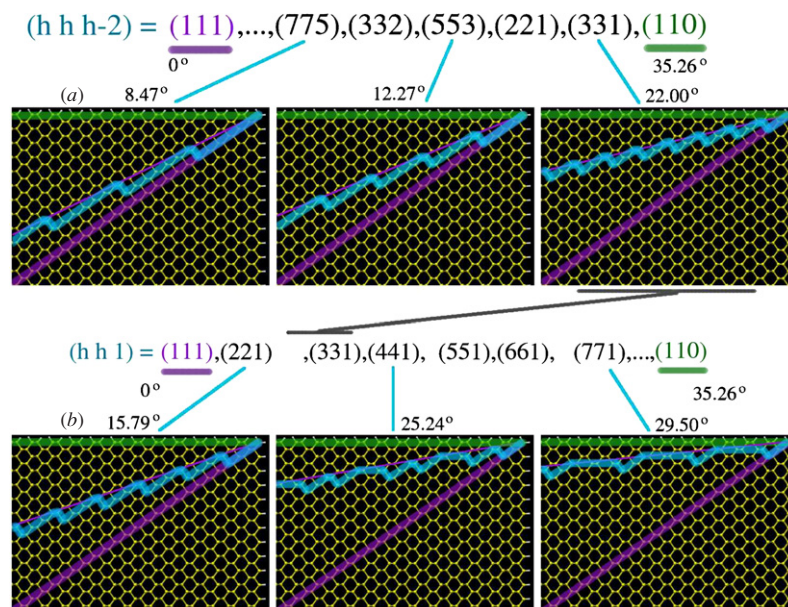
Figure 37. Crystallographic profile of the stepped surfaces between (1 1 1) and (1 1 0).
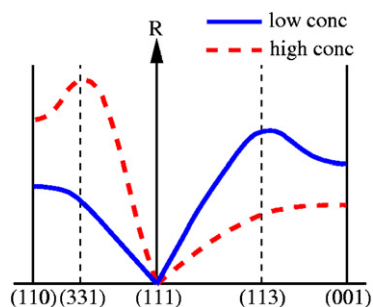
Figure 38. Typical variation of the etch rate at low and high concentration.

shows the overall expected variation of the etch rate between (1 1 1), (1 1 0) and (1 0 0) at low and high concentrations.

7. Conclusions

We have presented a simplified model of anisotropic etching of crystalline silicon for the three principal orientations (1 1 1), (1 1 0) and (1 0 0), including their vicinal surfaces. The model uses pit nucleation and step flow as the key atomistic processes in order to explain the different surface morphologies and exploits diffusion and micromasking phenomena as necessary ingredients responsible for major morphologic changes at low and high concentration.

The major conclusion is that the basic, *a priori* unrelated, morphologic features of (1 1 0) and (1 0 0), namely, the elongated zigzag structures and shallow round pits, respectively, are most likely due to the same mechanism: the formation of inhomogenous regions in the etchant. The apparent difference between the two morphologies is due to the underlying different crystallographic symmetry of the two surfaces. Although we have provided computational evidence for (1 1 0), similar simulations for (1 0 0) need to be realized in the near future. In addition, we are currently performing experiments to analyze the impact of diffusion on the morphology of (1 1 0) and (1 0 0) which will ultimately prove (or disprove) the conclusions from the simulations.

Another major conclusion of the paper is that the formation of pyramidal and trapezoidal hillocks on (1 1 0) and (1 0 0) at different concentrations is a related process which involves the fulfillment of four conditions, namely, apex micromasking, medium edge stability, strong facet stability and fast propagation of the floor surface.

The paper describes the change in the shape of the etch pits on (1 1 1) with concentration as the result of an underlying change in the relative reactivity of the SM and SD sites. We support the idea that the change in the relative reactivity of the two species can be due to a selective blocking mechanism by the etchant cations.

The basic morphology of the stepped (1 1 1) surfaces directly results from the underlying step propagation process. We have paid particular attention to the formation of polygonal steps on these surfaces, which can be explained not only by micromasking, as traditionally accepted, but also by the formation of inhomogenous regions in the etchant due to diffusion transport.

The particular effects of Cu as a micromasking agent according to previous experiments have been discussed. According to preliminary calculations, Cu preferentially pins silicon atoms at dihydride step sites as well as kink sites. This qualitatively explains the changes in morphology and etch rate observed experimentally.

Work is currently in progress in order to obtain a non-subjective, quantitative explanation of the role of Cu and other metal impurities as pinning agents. The results of the *ab initio* calculations will be presented in a forthcoming publication linking theory and experiment by means of Monte Carlo simulations of the Cu adsorption and desorption process. Once completed we will turn our attention to the adsorption of Pb and the puzzling effects of Mg, which can cancel out the effects of Cu [72].

We also aim at a more detailed explanation of the role of the etchant cations by means of Monte Carlo and *ab initio* simulations. In particular, we would like to understand the underlying mechanism for the rotation of the etch pits on (1 1 1) with concentration, which we have related in this paper to the chemical interaction between the surface-terminating hydroxyls and the cations, giving rise to selective blocking of the SD sites. In this respect, we feel the need to explore the similarities between the cation blocking mechanism and the use of electrochemical potentials during etching, both of which result in a similar etch pit rotation on (1 1 1) or, as referred to in the electrochemical studies, a similar 'step anisotropy reversal' [73]. The fact that the relative stability of the step monohydride and step dihydride sites can be controlled with external potentials as well as with concentration strongly suggests a substantial level of involvement of the etchant cations in the process.

Finally, we also would like to see an improvement in the understanding of the surfactants and other etchant additives. Although it is currently believed that their smoothening effect is due to a combination of the site-blocking and wetting characteristics of the etching solution, involving changes in the diffusion transport properties of the boundary layer and in the lifetime of hydrogen bubbles attached to the surface, it is necessary to determine more precisely the chemical and/or physical nature of blocking and the extent of the contribution from the diffusion processes. For this purpose, we are considering the use of *ab initio* and Monte Carlo simulations as well as performing new experiments.

References

[1] Allongue P, Brune H and Gerischer H 1992 *Surf. Sci.* **275** 414–23

[2] Elwenspoek M 1993 *J. Electrochem. Soc.* **140** 2075–80
[3] Allongue P, Costa-Kieling V and Gerischer H 1993 *J. Electrochem. Soc.* **140** 1009–18
[4] Hines M A, Chabal Y J, Harris T D and Alexander L 1994 *J. Chem. Phys.* **101** 8055–72
[5] Kasparian J, Elwenspoek M and Allongue P 1997 *Surf. Sci.* **388** 50–62
[6] Flidr J, Huang Y C, Newton T A and Hines M A 1998 *J. Chem. Phys.* **108** 5542–53
[7] van Veenendaal E, Nijdam A J, van Suchtelen J, Sato K, Gardeniers J G E, van Enckevort W J P and Elwenspoek M 2000 *Sensors Actuators* **84** 324–9
[8] Schröder H, Obermeier E, Horn A and Wachutka G K M 2001 *J. Microelectromech. Syst.* **10** 88–97
[9] Gosálvez M A, Kilpinen P, Haimi E, Nieminen R M and Lindroos V 2001 *Appl. Surf. Sci.* **178** 7–26
[10] Huang Y C, Flidr J, Newton T A and Hines M A 1998 *Phys. Rev. Lett.* **80** 4462–5
[11] Huang Y C, Flidr J, Newton T A and Hines M A 1998 *J. Chem. Phys.* **109** 5025–35
[12] Garcia S P, Bao H and Hines M A 2004 *Phys. Rev. Lett.* **96** 166102
[13] Garcia S P, Bao H and Hines M A 2004 *J. Phys. Chem.* B **108** 6062–71
[14] Camon H, Danel J S and Djafari-Rouhani M 1992 *Sensors Actuators* A **33** 103–5
[15] Camon H and Moktadir Z 1995 *Sensors Actuators* A **46-47** 27–9
[16] Camon H, Moktadir Z and Djafari-Rouhani M 1996 *Mater. Sci. Eng.* B **37** 142–5
[17] Camon H and Moktadir Z 1997 *Microelectron. J.* **28** 509–17
[18] Tan O and Büttgenbach S 1994 *Sensors Actuators* A **45** 85–9
[19] Büttgenbach S and Tan O 1996 *Proc. of IEEE European Design and Test Conf. (ED & TC 1996)* (Los Alamitos, CA: IEEE Computational Soc. Press) pp 454–8
[20] Zhu Z and Liu C 2000 *Comput. Model. Eng. Sci.* **1** 11–9
[21] Zhou Z-F, Huang Q-A, Li W-H and Zhu C 2006 *J. Physics: Conf. Ser.* **34** 674–9
[22] Burton W K, Cabrera N and Frank F C 1951 *Phil. Trans. R. Soc.* A **243** 299–358
[23] Krug J 2005 *Multiscale Modelling of Epitaxial Growth* vol 149 ed A Voigt (Basel: Birkhäuser) p 69
[24] Price J B 1973 Semiconductor silicon *The Electrochemical Society Softbound Proceedings Series* ed H R Huff and R R Burgess (Princeton, NJ: Electrochemical Society) pp 339–53
[25] Seidel H, Csepregi L, Heuberger A and Baumgartel H 1990 *J. Electrochem. Soc.* **137** 3612–26
[26] Abu-Zeid M M, Kendall K L, de Guel G R and Galeazzi R 1985 *Spring Conf. of the Electrochem. Soc., Extended Abstracts (Toronto, ON, Canada, 12–17 May)* vol 85 p 400 (Abstract 275)
[27] Shikida M, Sato K, Tokoro K and Uchikawa D 2000 *Sensors Actuators* A **80** 179–88
[28] Tan S, Boudreau R and Reed M 2001 *Sensors Mater.* **13** 303–13
[29] Gosálvez M A, Xing Y, Hynninen T, Uwaha M, Foster A S, Nieminen R M and Sato K 2007 *J. Micromech. Microeng.* **17** S27–37
[30] Campbell S A, Cooper K, Dixon L, Earwaker R, Port S N and Schiffrin D J 1995 *J. Micromech. Microeng.* **5** 209–18
[31] Baum T and Schiffrin D J 1997 *J. Micromech. Microeng.* **7** 338–42
[32] Baum T, Satherley J and Schiffrin D J 1998 *Langmuir* **14** 2925–8
[33] Schröder H, Obermeier E and Steckenborn A 1999 *J. Micromech. Microeng.* **9** 139–45
[34] Tan S S, Reed M L, Han H and Boudreau R 1996 *J. Microelectromech. Syst.* **5** 66–72
[35] Dorsch O, Hein A and Obermeier E 1997 *Dig. of Tech. Papers Transducers 97 (Chicago, IL, USA, 16–17 June)* pp 683–6

[36] Nijdam A J, van Veenendaal E, Cuppen H M, van Suchtelen J, Reed M L, Gardeniers J G E, van Enckevort W J P, Vlieg E and Elwenspoek M 2001 *J. Appl. Phys.* **89** 4113–23
[37] van Veenendaal E, Sato K, Shikida M, Nijdam A J and van Suchtelen J 2001 *Sensors Actuators* A **93** 232–42
[38] Landsberger L M, Naseh S, Kahrizi M and Paranjape M 1996 *J. Microelectromech. Syst.* **5** 106–16
[39] Hein A, Dorsch O and Obermeier E 1997 *Dig. of Tech. Papers Transducers 97 (Chicago, IL, USA, 16–17 June)* pp 687–90
[40] Tanaka H, Abe Y, Yoneyama T, Ishikawa J, Takenaka O and Inoue K 2000 *Sensors Actuators* A **82** 270–3
[41] Tanaka H, Abe Y and Inoue K 2002 *Proc. 3rd Workshop on Physical Chemistry of Wet Etching of Silicon (Nara, Japan, 4–6 June)* ed K Sato pp 58–61
[42] Tanaka H, Cheng D, Shikida M and Sato K 2006 *Sensors Actuators* A **128** 125–31
[43] Gosálvez M A and Nieminen R M 2003 *New J. Phys.* **5** 100
[44] van Suchtelen J and van Veenendaal E 2000 *J. Appl. Phys.* **87** 8721–31
[45] van Veenendaal E, van Suchtelen J, van Enckevort W J P, Sato K, Nijdam A J, Gardeniers J G E and Elwenspoek M 2000 *J. Appl. Phys.* **87** 8732–40
[46] Gosálvez M A 2003 Atomistic modeling of anisotropic etching of crystalline silicon *Doctoral Dissertation 123* Laboratory of Physics, Helsinki University of Technology http://lib.hut.fi/Diss/2003/isbn9512267071
[47] Divan R, Moldovan N and Camon H 1999 *Sensors Actuators* A **74** 18–23
[48] Yang C-R, Chen P-Y, Chiou Y-C and Lee R-T 2005 *Sensors Actuators* A **119** 263–70
[49] Yang C-R, Chen P-Y, Yang C-H, Chiou Y-C and Lee R-T 2005 *Sensors Actuators* A **119** 271–81
[50] Resnik D, Vrtacnik D, Aljancic U, Mozek M and Amon S 2005 *J. Micromech. Microeng.* **15** 1174–83
[51] Cheng D, Gosálvez M A, Hori T, Sato K and Shikida M 2006 *Sensors Actuators* A **125** 415–21
[52] Merlos A, Acero M, Bao M H, Baussells J and Esteve J 1993 *Sensors Actuators* A **37-38** 737–43
[53] Zubel I and Kramkowska M 2001 *Sensors Actuators* A **93** 138–47
[54] Zubel I and Kramkowska M 2004 *Sensors Actuators* A **115** 549–56
[55] Hines M A 2003 *Ann. Rev. Phys. Chem.* **54** 29–56
[56] Gosálvez M A, Cheng D, Nieminen R M and Sato K 2006 *New J. Phys.* **8** 269
[57] Allongue P 1996 *Phys. Rev. Lett.* **77** 1986–9
[58] Allongue P, Kieling V and Gerischer H 1995 *Electrochim. Acta* **40** 1353–60
[59] Xia X H and Kelly J J 2000 *Electrochim. Acta* **45** 4645–53
[60] Bressers P M M C, Pagano S A S P and Kelly J J 1995 *J. Electroanal. Chem.* **391** 159–68
[61] Haiss W, Raisch P, Schiffrin D J, Bitsch L and Nichols R J 2002 *Faraday Discuss.* **121** 167–80
[62] Tabata O 2001 *Sensors Mater.* **13** 271–83
[63] Higashi G S, Chabal Y J, Trucks G W and Raghavachari K 1990 *Appl. Phys. Lett.* **56** 656–8
[64] Hines M A, Chabal Y J, Harris T D and Harris A L 1994 *J. Chem. Phys.* **101** 8055–72
[65] Jakob P and Chabal Y J 1991 *J. Chem. Phys.* **95** 2897–909
[66] Cheng D, Gosálvez M A, Shikida M and Sato K 2006 *Proc. MEMS 2006, The 19th IEEE Int. Conf. on Micro Electro Mechanical Systems (Istanbul, Turkey, 22–26 Jan 2006)* pp 318–21
[67] Tanaka H, Yamashita S, Abe Y, Shikida M and Sato K 2004 *Sensors Actuators* A **114** 516–20
[68] Zubel I, Barycka I, Kotowska K and Kramkowska M 2001 *Sensors Actuators* A **87** 163–71

[69] Sato K, Masuda T and Shikida M 2002 *Proc. 3rd Workshop on Physical Chemistry of Wet Etching of Silicon (Nara, Japan, 4–6 June)* ed K Sato pp 43–46

[70] Tan S S, Reed M L, Han H and Boudreau R 1996 *J. Microelectromech. Syst.* **4** 147–55

[71] Singh P K, Kumar R, Lal M, Singh S N and Das B K 2001 *Sol. Energy Mater. Sol. Cells* **70** 103–13

[72] Tanaka H 2005 High-speed anisotropic wet etching of silicon and the effects of metal impurities in KOH solution *PhD Thesis* Nagoya University, Nagoya, Japan

[73] Nguyen Q D and Elwenspoek M *Proc. Fifth Int. Workshop on Physical Chemistry of Wet Etching of Semiconductors, PCWES 2006 (Saarbrücken, Germany, June 19–21, 2006)* ed H Seidel pp 8–9